

# Robust normality transformation for outlier detection in diverse distributions, with application to functional neuroimaging data

Fatma Parlak<sup>1,2\*</sup>, Saranjeet Singh Saluja<sup>1,\*</sup>, Amanda Mejia<sup>1</sup>

<sup>1</sup>Department of Statistics, Indiana University Bloomington, USA

<sup>2</sup>Department of Mathematics, Ankara Yıldırım Beyazıt University, Turkey

\*These authors contributed equally to this work.

## Abstract

Automatic detection of statistical outliers is facilitated through knowledge of the source distribution of regular observations. Since the population distribution is often unknown in practice, one approach is to apply a transformation to Normality. However, the efficacy of transformation is hindered by the presence of outliers, which can have an outsized influence on transformation parameter(s) and lead to masking of outliers post-transformation. Robust Box-Cox and Yeo-Johnson transformations have been proposed but those transformations are only equipped to deal with skew. Here, we develop a novel robust method for transformation to Normality based on the highly flexible sinh-arcsinh (SHASH) family of distributions, which can accommodate skew, non-Gaussian tail weights, and combinations of both. A critical step is initializing outliers, given their potential influence on the highly flexible SHASH transformation. To this end, we consider conventional robust z-scoring and a novel anomaly detection approach. Through extensive simulation studies and real data analyses representing a wide variety of distribution shapes, we find that SHASH transformation outperforms existing methods, exhibiting high sensitivity to outliers even at heavy contamination levels (20-30%). We illustrate the utility of SHASH transformation-based outlier detection in the context of noise reduction in functional neuroimaging data.

# 1 Introduction

Outliers are data observations that are significantly different from the majority or bulk of the data. They may arise from a different source distribution or be due to artifacts or data entry errors. The presence of outliers can compromise statistical models, which typically assume that data observations or model errors are identically distributed. In addition, outliers often have a strong influence on model fitting, resulting in potentially misleading results and erroneous conclusions. It is therefore vital to either use estimation techniques robust to the presence of outliers, such as rank-based methods, or to detect and appropriately address outliers prior to model estimation.

One of the principal challenges in outlier detection methodology is to avoid the influence of outliers themselves in the detection process Rousseeuw and Hubert (2011). For instance, in linear regression it is well-known that certain types of outliers can have a dramatic influence on the regression fit, essentially pulling the regression line towards themselves and shrinking their residuals. Similarly, distance-based outlier detection methods require center and scale values, non-robust estimators of which are likely to be influenced by outlying observations, leading to underestimation of the true distances of those same observations. These distortions can lead to *masking*, where true outliers go undetected, or *swamping*, where regular observations falsely appear to be outliers (Hawkins, 1980). Thus, robust methods are essential for accurate outlier detection.

Fortunately, there is a long literature on robust estimation of center and scale in both the univariate (Hampel, 1974; Rousseeuw and Croux, 1993) and multivariate (Maronna, 1976; Donoho, 1982; Rousseeuw, 1984; Maronna and Zamar, 2002) settings. Thus, it is generally easy and efficient to compute robust distances with well-established theoretical properties. For instance, the multivariate minimum covariance determinant (MCD) distance has high breakdown point, is relatively statistically efficient, is asymptotically Normal, and is fast to compute (Rousseeuw and Driessen, 1999). In the univariate setting, the problem is even simpler since it only requires a good estimator of two parameters, the location (e.g., median) and scale (e.g., median absolute deviation).

Once a robust z-score or distance has been computed, the only thing left to do is threshold it to flag outliers. When choosing a threshold, the objective is to detect all true outliers (high sensitivity), while leaving non-outlying observations alone (high specificity). While conceptually simple, this is not always an easy task. Consider first the ideal scenario of Normally distributed data. Computing

a z-score transforms the data to central normality if our estimates of center and scale are good, at which point we can choose a threshold using quantiles of the  $N(0, 1)$  distribution. For instance, if we choose the 0.005 and 0.995 quantiles as our lower and upper thresholds, the most extreme 1% of non-outlying observations will be falsely labeled as outliers, i.e. *false positives*. In the case of multivariate Gaussian data, Hardin and Rocke (2005) showed that MCD distances approximately follow a scaled F distribution. Adopting the 0.99 quantile of that distribution as an outlier detection threshold would similarly lead to an expected false positive rate of 1%.

However, if our data is not Normally distributed, the choice of appropriate threshold is less straightforward. In practice, it is somewhat rare for population data to follow a Gaussian distribution. In this case, one can either adopt methods suitable for non-Gaussian data, such as non-parametric methods, or apply a transformation to make the assumption of Gaussianity reasonable. Transformation to standard normality greatly simplifies the problem of outlier detection in both univariate and multivariate data, using the techniques described above. The problem is that transformation involves the estimation of certain parameters, which must be done in a way robust to the presence of outliers to avoid their influence.

One well-known family of transformations is the Box-Cox power transformations (Tukey, 1957; Box and Cox, 1964) for positive-valued data or Yeo-Johnson (YJ) transformation (Yeo and Johnson, 2000) for real-valued data. Recently, Raymaekers and Rousseeuw (2021) developed a robust transformation to central normality based on Box-Cox and YJ transformation. Briefly, an iterative maximum likelihood estimation (MLE) procedure is used, which excludes certain observations likely to represent outliers at each iteration. These observations are initialized by standardizing the data using robust estimates of center and scale, i.e. computing a robust z-score, and applying standard Gaussian quantile cutoffs. After transformation at each iteration, the same Gaussian quantile cutoffs are applied. To our knowledge, this is the first robust technique for transformation to normality in the literature, and was shown to effectively transform the data and isolate outlying observations in the presence of skew and a small number of outliers.

However, two main drawbacks limit the application of robust Box-Cox or YJ transformation in a broad array of settings. First, those transformations are designed for skewed data and cannot address heavy tails, short tails, or combinations of non-Gaussian features. Second, the use of robust z-scoring to initialize the algorithm may fail when the proportion of outliers in the data is high. This

is because (a) this is designed to work on data that is close to Normally distributed, which the data is in general not at the initialization stage, and (b) the robust scale estimate and even the location estimate may be contaminated with high rates of outliers, as we will demonstrate. Since outliers can be highly influential in the transformation, failure to exclude outliers from the initial transformation parameter estimation may lead to a strong influence of outliers on the transformation, and ultimately low sensitivity to outliers post-transformation. In our simulation studies, we indeed find that the sensitivity of robust Box-Cox or YJ transformation suffers when there are more than a few outliers.

In this paper, we develop a novel robust transformation to central normality applicable to diverse distributions, which overcomes the two limitations above. To address the first limitation, we consider transformations that can address both tail weight and skew. In recent years, several transformations to normality have been developed that can handle skew as well as tail weight (Jones and Pewsey, 2009; Goerg, 2015; Tsai et al., 2017). Here, we adopt the highly flexible sinh-arcsinh (SHASH) family of distributions and associated transformation, which can address skew, non-Gaussian tailweight, and combinations of both Jones and Pewsey (2009). To address the second limitation, namely initialization of outliers, we consider alternatives to robust z-scoring, which fails in many settings, as we will show. Specifically, we propose a novel variation of nonparametric anomaly detection, bridging the statistical and machine learning outlier detection literatures.

The remainder of the paper proceeds as follows. In section 2, we introduce the SHASH family of distributions and the SHASH transformation, and we describe the robust SHASH transformation and outlier initialization procedures. In section 3, we present extensive simulation studies using a wide array of distribution shapes and outlier contamination levels to assess the performance of robust SHASH transformation for outlier detection, compared with existing techniques including robust z-scoring and robust Box-Cox/YJ transformation. In section 4, we apply the proposed and existing techniques to several real world datasets to compare their performance in different scenarios. Finally, in section 5, we apply SHASH-based outlier detection to the problem of noise reduction in functional neuroimaging data to illustrate its utility in an important scientific context. We conclude with a discussion of our findings, as well as limitations and directions for future research.

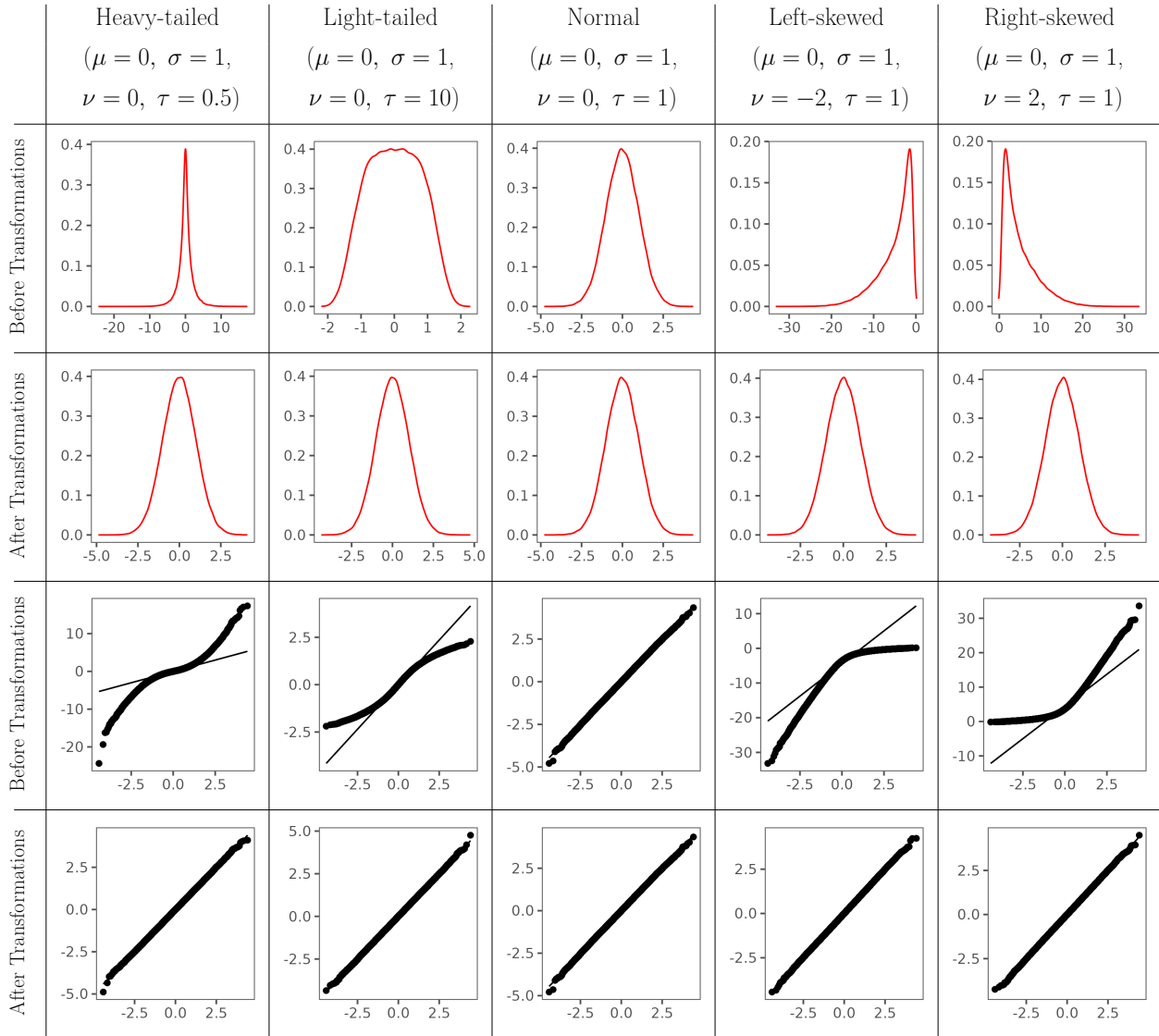


Figure 1: **Example SHASH random variables and their transformation to Normality.** Each data set contains 100000 randomly sampled draws from a SHASH distribution with given parameter values. These represent a variety of distributional shapes: heavy-tailed, light-tailed, Normal, left-skewed, and right-skewed, respectively. For each random variable, an estimated density curve and Normal QQ plot before and after transformation to Normality is shown, illustrating how SHASH random variables can be transformed to standard Normal random variables.

## 2 Methods

### 2.1 The SHASH distribution family and transformation

The sinh-arcsinh (SHASH) family of distributions is a versatile family characterized by four parameters controlling the mean ( $\mu$ ), variance ( $\sigma$ ), skewness ( $\nu$ ), and tailweight ( $\tau$ ) (Jones and Pewsey, 2009). Its most basic form has only two parameters,  $\nu$  and  $\tau$ , and arises by applying an inverse SHASH transformation to a standard Normal random variable. Letting  $Z$  be standard Normal random variable,  $X = S_{\nu,\tau}^{-1}(Z)$  is said to follow a SHASH distribution with parameters  $\nu$  and  $\tau$ . The SHASH transformation  $S_{\nu,\tau}$  and its inverse  $S_{\nu,\tau}^{-1}$  are defined as

$$Z = S_{\nu,\tau}(X) = \sinh [\tau \sinh^{-1}(X) - \nu] \quad (1)$$

$$X = S_{\nu,\tau}^{-1}(Z) = \sinh [\tau^{-1}(\sinh^{-1}(Z) + \nu)]. \quad (2)$$

By a change of variables, the density function of a 2-parameter SHASH distribution is

$$f_X(x|\nu, \tau) = \tau \left( \frac{1 + (S_{\nu,\tau}^2(x))}{2\pi(1 + x^2)} \right)^{-\frac{1}{2}} \exp \left( \frac{-S_{\nu,\tau}^2(x)}{2} \right). \quad (3)$$

The four-parameter family arises by incorporating location and scale parameters  $\mu$  and  $\sigma$ . Under regularity conditions of the maximum likelihood theory, Jones and Pewsey (2009) demonstrated that the estimation of the mean is asymptotically independent of the scale and tailweight parameters, but the scale and tailweight parameters are asymptotically dependent. They alleviate this issue through a reparameterization, replacing  $\sigma$  with  $\sigma\tau$ . The four-parameter SHASH transformation and its inverse are given by

$$Z = S_{\mu,\sigma,\nu,\tau}(X) = \sinh \left[ \tau \sinh^{-1} \left( \frac{X - \mu}{\sigma\tau} \right) - \nu \right] \quad (4)$$

$$X = S_{\mu,\sigma,\nu,\tau}^{-1}(Z) = \sigma\tau \sinh \left[ \tau^{-1} \sinh^{-1}(Z) + \nu \right] + \mu. \quad (5)$$

This leads to what is known as the SHASHo2 distribution (hereafter ‘‘SHASH’’) implemented in the `gamlss.dist` R package Rigby et al. (2019). Its probability density function, using the identities

Parameter	Range	Function
$\mu$	$-\infty < \mu < \infty$ ,	modulates the mean
$\sigma$	$0 < \sigma < \infty$ ,	modulates the variance
$\nu$	$-\infty < \nu < \infty$ ,	modulates the skewness
$\tau$	$0 < \tau < \infty$ ,	modulates the tailweight

Table 1: Range and role of each parameter in the SHASH( $\mu, \sigma, \nu, \tau$ ) family of distributions.

$\sinh(x) = (e^x - e^{-x})/2$  and  $\cosh(x) = (e^x + e^{-x})/2$ , is (see Appendix A for derivation):

$$f_X(x|\mu, \sigma, \nu, \tau) = \frac{c(x)\tau}{\sqrt{2\pi\sigma^2(1 + ((x - \mu)/\sigma\tau)^2)}} \exp\left(-\frac{r^2(x)}{2}\right) \quad (6)$$

where  $r(x)$  and  $c(x)$  are given by

$$r(x) = \frac{1}{2} \left\{ \exp\left[\tau \sinh^{-1}\left(\frac{x - \mu}{\sigma\tau}\right)\right] - \exp\left[-\nu \sinh^{-1}\left(\frac{x - \mu}{\sigma\tau}\right)\right] \right\} \quad (7)$$

$$c(x) = \frac{1}{2} \left\{ \exp\left[\tau \sinh^{-1}\left(\frac{x - \mu}{\sigma\tau}\right)\right] + \exp\left[-\nu \sinh^{-1}\left(\frac{x - \mu}{\sigma\tau}\right)\right] \right\}. \quad (8)$$

The range and role of each parameter are given in **Table 1**. To illustrate the influence of each parameter on the distribution shape, **Figure 1** shows five different distributions in the SHASH family, including heavy tailed, light tailed, Normal, left skewed and right skewed. In the top row, density curves for each distribution are shown. Comparing the heavy-tailed and light-tailed distributions,  $\tau$  is the only parameter that changes: the value increases from 0.5 to 10, illustrating that higher values ( $\tau > 1$ ) produce heavier tails while lower values ( $\tau < 1$ ) produce lighter tails. Similarly, comparing the left-skewed and right-skewed distributions,  $\nu$  is the only parameter that changes, from  $-2$  to  $2$ . Negative values of  $\nu$  produce a left-skewed distribution, while positive values produce a right-skewed distribution.

Recall that SHASH random variables are transformed to standard normality by applying the SHASH transformation given in equation 4. The second row of **Figure 1** displays the density curves after applying the SHASH transformation with the corresponding parameters. The last two rows show Normal quantile-quantile (Q-Q) plots before and after transformation. After applying the SHASH transformation with correct parameter values, each distribution clearly follows a standard Normal distribution.

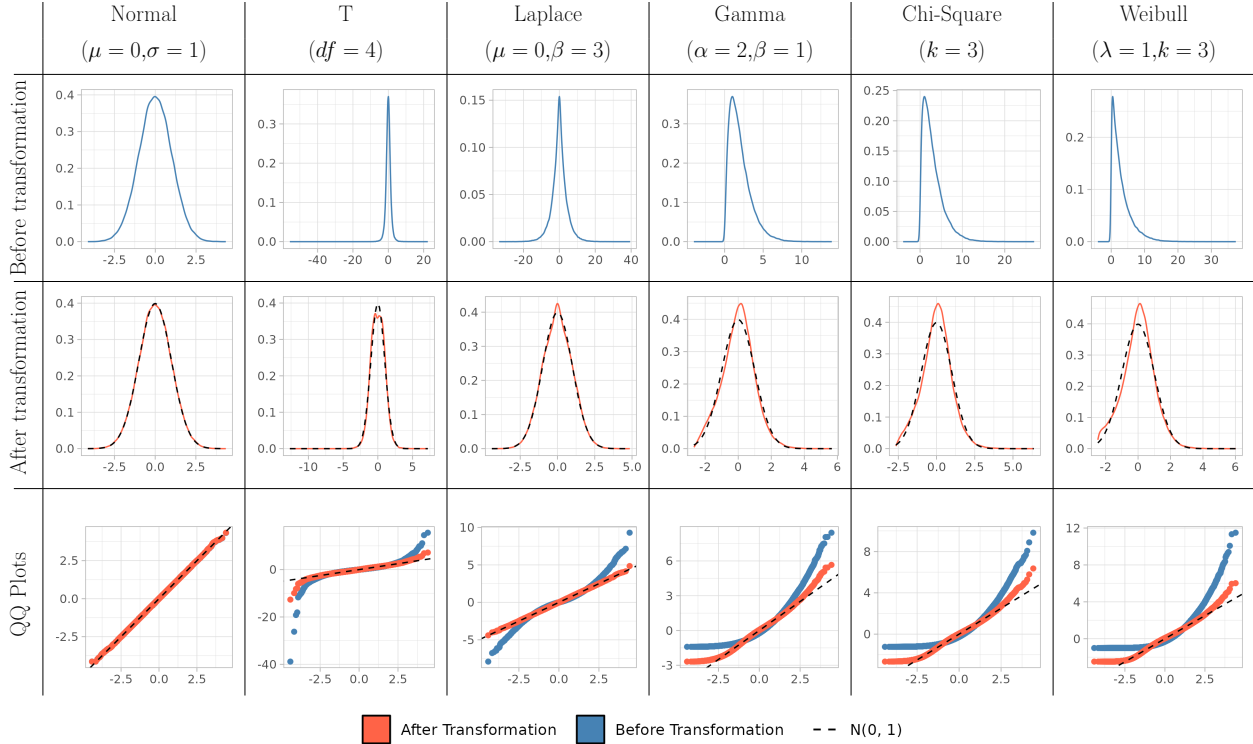


Figure 2: **Illustration of applying SHASH transformation to non-SHASH distributions.** Each distribution was modeled as a SHASH random variable, although most distributions shown here do not fall within the SHASH family of distributions. The bottom panel shows the distributions after applying SHASH transformation using maximum likelihood estimates of the SHASH parameters. While only the Normal distribution is perfectly transformed, the other example distributions become much closer to Normal than before transformation.

Our proposed transformation assumes that the underlying data can be modeled using a SHASH distribution. This may be reasonable in many settings even when the data does not actually arise from a SHASH distributions given the flexibility of the SHASH family to represent widely diverse distributional shapes. **Figure 2** illustrates the use of the SHASH transformation on several different well-known distributions. Whereas in Figure 1 the SHASH parameters were known, here we estimate them via maximum likelihood. With the exception of the Normal distribution, none of these distributions actually falls within the SHASH family, yet applying the SHASH transformation using estimated parameters brings all of them much closer to Normality. The transformation is strikingly accurate for the Laplace distribution, which resembles the SHASH heavy tailed distribution shown in Figure 1. The  $t$  distribution retains some heaviness in the tails after transformation, but much less than prior to transformation. The three skewed distributions all retain some degree of skew, but it is strongly mitigated by transformation, especially in the right tail where outliers may present.

## 2.2 Robust SHASH transformation

Robust SHASH transformation and outlier detection involves the following steps, implemented in the open source `rrobot` R package.

1. Initialize outlier labels using existing robust techniques, described below.
2. Model the data using a SHASH distribution, using MLE to obtain SHASH parameter estimates (Rigby et al., 2019), excluding observations currently labeled as outliers.
3. Apply SHASH transformation (equation 4) using the estimated parameters.
4. Update outlier labels as observations whose transformed values exceed a certain threshold.
5. Iterate steps 2-4, excluding previously identified outliers from parameter estimation, until convergence, defined as no change in the identified set of outlier observations.
6. Apply a final outlier detection threshold to the transformed data.

Here we adopt a final outlier detection threshold of  $\pm 3$ , or  $+3$  if the original data is strictly positive. If the transformation is successful at achieving standard Normality, a threshold of  $\pm 3$  should result in a false positive rate of 0.003%. Depending on the context, a more aggressive threshold or a more lenient threshold can be adopted in order to prioritize maximizing power to detect outliers or minimizing false positives.

This procedure follows the same general strategy as Raymaekers and Rousseeuw (2021) for Box-Cox and YJ transformations, but uses the more flexible SHASH transformation and considers alternative outlier initialization methods. Outlier initialization is a crucial step for any transformation, but especially so here given the high degree of flexibility of the SHASH transformation. If outliers are allowed to influence the SHASH parameter estimates, they are likely to have a strong effect and cause masking of true outliers.

Specifically, we consider two outlier initialization methods: robust  $z$ -scoring and a novel anomaly detection approach. For robust  $z$ -scoring, a  $z$ -score is computed by subtracting a robust estimate of location and dividing by a robust estimate of scale. We use the median,  $m_x$ , and the median absolute deviation,  $MAD_x = 1.4826 \text{ med}(|x_i - m_x|)$ , which is consistent for the standard deviation under Gaussianity (Ruppert, 2010, p. 118). Observations exceeding the standard Normal 0.995

quantile or below the 0.005 quantile, equal to  $\pm 2.58$  (or simply exceeding 2.58 if the original data is strictly positive), are initialized as outliers, as in Raymaekers and Rousseeuw (2021).

While robust z-scoring works well in certain cases, its performance breaks down in skewed distributions and in the presence of many outliers, as our simulation studies will show. Thus, we consider an alternative approach for initializing outliers. Isolation forest (iForest) is a tree-based anomaly detection algorithm that identifies outliers by recursively isolating data points (Liu et al., 2008). The key idea is that outliers are more susceptible to isolation and therefore require fewer splits. Each data point is assigned an anomaly score between 0 and 1, where values closer to 1 indicate a higher likelihood of being an outlier. Anomaly score thresholds between 0.5 and 0.6 are commonly considered in the literature (Liu et al., 2008; Chabchoub et al., 2022), but to our knowledge there exists no principled method of selecting a score threshold. Here, we propose a variant of iForest tailored for univariate settings where outliers assume extreme values. We first identify the smallest-magnitude value identified as an anomaly with iForest, based on a threshold of 0.6 as recommended by Liu et al. (2008), and adopt its value as the outlier threshold. That is, all observations larger than the smallest anomaly are labeled as outliers. In the case of real-line support, this is applied in both tails.

The complete SHASH pipeline using robust z-scoring for outlier initialization is referred to as SHASH-z, and the pipeline using our iForest variation for outlier initialization as SHASH-i.

### 3 Simulation Studies

To evaluate the performance of SHASH-based outlier detection across a wide range of scenarios, we perform extensive simulation studies wherein the true outliers are known. For comparison, we apply two existing methods: robust z-scoring and robust Box-Cox/YJ transformation (Raymaekers and Rousseeuw (2021)). For all methods, we use a final outlier detection threshold of  $\pm 3$  (or  $+3$  for positively valued data).

We consider data arising from several parametric distributions and vary the degree of outlier contamination with outliers from light (1%) to heavy (30%). We consider two main categories of distributions: (1) symmetric distributions with support on  $(-\infty, \infty)$  and (2) right-skewed distributions with support on  $(0, \infty)$ . Table 2 lists the distributions, their parameter values, and the

Support	Distribution	Parameters	Purpose
$\mathbb{R}$	Normal( $\mu, \sigma$ )	$\mu = 0, \sigma = 1$	Optimal case for all methods
	Student's $t(\nu)$	$\nu = 4$	Heavy-tailed
	Laplace( $\mu, \beta$ )	$\mu = 0, \beta = 3$	Exponential shape
$\mathbb{R}_+$	Gamma( $\alpha, \beta$ )	$\alpha = 2, \beta = 1$	Skewed with heavy tails
	Chi-square( $k$ )	$k = 3$	Skewed with heavier tails
	Weibull( $\lambda, k$ )	$\lambda = 1, k = 3$	Skewed with exponential shape

Table 2: Summary of distributions used in the simulation study, along with selected parameters and evaluation purpose.

rationale for their inclusion in the study. Since the robust empirical rule is designed for Normally distributed data, it is expected have better performance in symmetric versus asymmetric distributions and optimal performance for Gaussian data. Since robust YJ transformation is designed to deal with skew, it is expected to have better performance in skewed or Gaussian data and worse performance in heavy tailed or exponential distributions. For each scenario considered, we perform 100 independent simulation repetitions, each with a fixed sample size of  $n = 500$ .

### 3.1 Outlier Generation

We induce outliers by first transforming the distribution to be approximately Normal, then replacing a randomly selected fraction of each dataset with larger-magnitude values. For distributions defined on the real line, outliers are randomly assigned positive or negative signs. Figure 3 illustrates the outlier generation process for each type of distribution. The first column shows a random sample of 500 with no outliers. Using a separate large sample from the same distribution (100,000 observations), the data was modeled as a SHASH distribution and the MLEs of the SHASH parameters were obtained from that dataset. The second column shows the data after applying the SHASH transformation to approximately achieve standard Normality. The third column shows the transformed data after randomly replacing 10% of the observations with outliers. These outliers are generated as a scaled and shifted Chi-square distribution. Finally, as shown in the fourth column, the data contaminated with outliers is reverse-transformed back to the original distribution, returning the non-outlying observations to their original values.

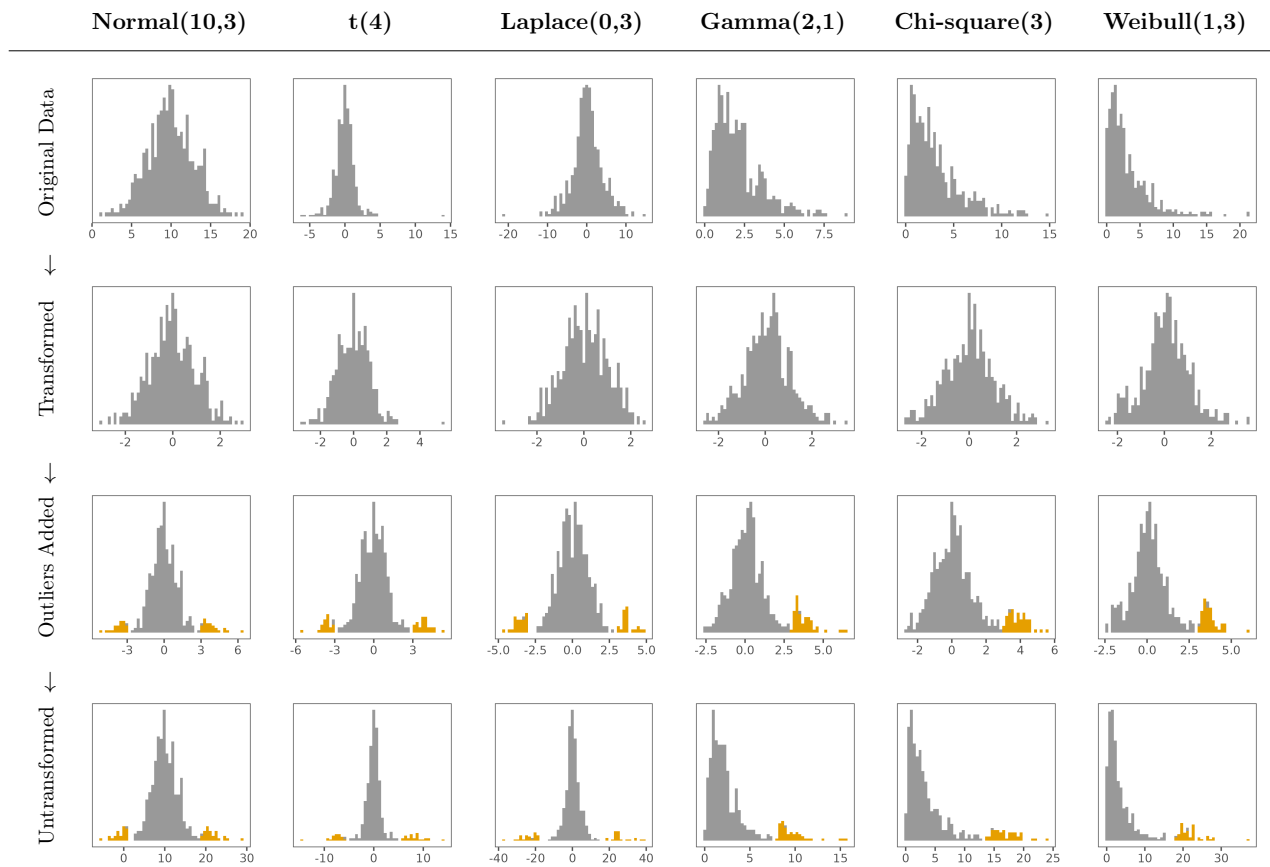


Figure 3: **The outlier contamination process for simulation studies.** The first row shows an original outlier-free sample. For the non-Gaussian distributions, the second row shows the same data after applying a SHASH transformation (with parameters estimated via MLE from the large sample shown in Figure 2) to approximately achieve standard Normality. For the Gaussian scenario, the data are simply standardized to mean zero and unit variance. In the third row, outliers are introduced by replacing  $x\%$  of the data (here 10%) with values randomly sampled as  $\chi^2(4)/5 + 3$ , as illustrated in the third row in orange. Finally, the fourth row shows the contaminated data reverse-transformed to the original scale and distribution.

## 3.2 Evaluation Metrics

The accuracy of outlier detection is evaluated by comparing the flagged outliers against the true outliers in each simulated dataset. Two performance metrics are used: the true positive rate (TPR), or sensitivity, and the false positive rate (FPR), or 1 - specificity. True positives (TP) are truly outlying observations that are correctly identified as outliers; false positives (FP) are truly non-outlying observations that have been incorrectly flagged as outliers. Likewise, true negatives (TN) are truly non-outlying observations correctly classified as non-outliers; false negatives (FN) are true outliers not identified as outliers. The true positive rate  $TPR = TP/(TP + FN)$  quantifies a method's sensitivity to actual outliers. A TPR close to 1.0 indicates that the method detects most of the true outliers. The false positive rate  $FPR = FP/(FP + TN)$  quantifies the proportion of truly non-outlying observations incorrectly identified as outliers. A low FPR indicates minimal misclassification of non-outlying data observations as outliers, i.e. high specificity. If the data is perfectly transformed to standard Normality, applying an outlier detection threshold of  $\pm 3$  should yield a false positive rate (FPR) of 0.003.

## 3.3 Simulation Results

### 3.3.1 Visualization of example datasets

**Figure 4** shows randomly selected examples for each of the six distributions considered in the simulation study at 10% outlier contamination. **Figures S.1 to S.6** show examples at different outlier contamination levels from 1% to 30%. The columns of each figure show the original data, the data after robustly z-scoring, after applying robust Box-Cox/YJ transformation, and after applying the robust SHASH-z and SHASH-i transformation. Vertical dashed lines indicate the outlier detection threshold(s), and true outliers are shown in red. After a successful transformation, the data should approximately follow a standard Normal distribution, and true outliers will fall outside the thresholds, while non-outliers will mainly fall within them.

Consider first the Gaussian case. If the data is known to follow a Normal distribution, then no transformation is needed. However, we may not have this knowledge a-priori, so by applying transformation to Normally-distributed data, we are evaluating whether there is a detrimental effect of transformation. At 10% outlier contamination, all methods perform well. However, Figure S.1

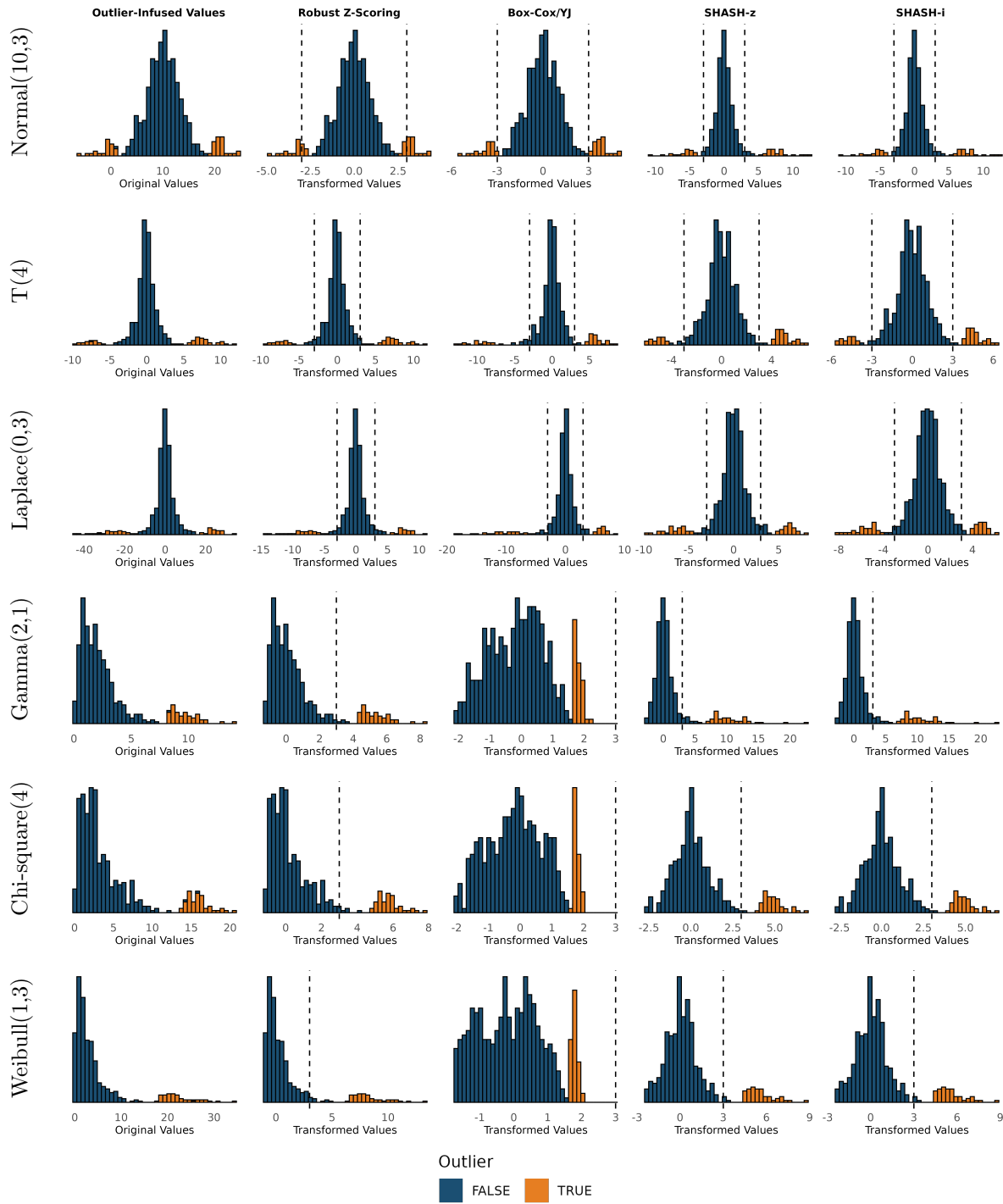


Figure 4: **Example histograms of transformed values by robust z-scoring, Box-Cox/YJ transformation, and SHASH transformation for 10% outlier contamination.** For each distribution, one randomly selected simulated dataset is shown. Vertical lines indicate the outlier detection thresholds, and true outliers are shown in orange. All methods perform fairly well, with the exception of robust Box-Cox/YJ transformation in the skewed distributions, where we see masking of all true outliers.

shows that at higher outlier contamination, robust z-scoring tends to fail, as well as Box-Cox/YJ transformation and SHASH-z transformation. Since those methods depend on robust z-scoring for initial outlier detection, they are likely failing due to influence of outliers not initially flagged. By contrast, SHASH-i transformation is seen to work quite well, even at 30% outlier contamination.

Turning to the  $t$  and Laplace distributions, examining Figure 4 we see that both robust z-scoring and Box-Cox/YJ transformation misclassify some non-outliers as outliers due to their heavy tails. The Box-Cox/YJ transformation is not equipped to transform heavy tailed distributions to Normality, since it is designed to eliminate skew. For both the  $t$  and Laplace distributions, in these examples, the SHASH transformations reduce the tailweight and largely avoid misclassification of regular observations as outliers.

For skewed distributions, Figure 4 shows that at 10% outlier contamination, both SHASH-z and SHASH-i transformation achieve near symmetry, with outliers far into the right tail. Although some regular observations are still misclassified as outliers, they are generally fewer than prior to transformation. The performance of robust z-scoring is, as expected, less than perfect, with several regular observations in the tail misclassified as outliers. However, at higher outlier contamination levels shown in Figures S.4 to S.6, robust z-scoring is often seen to fail. That in turn causes Box-Cox/YJ and SHASH-z to fail, since they rely on robust z-scoring for outlier initialization. SHASH-i, by contrast, performs quite reasonably even up to 30% outlier contamination.

Quite surprisingly, Box-Cox/YJ transformation seems to consistently fail even at 5-10% outlier contamination for all the three skewed distributions, with true outliers falling well below the outlier detection threshold. This indicates masking of outliers due to their influence on the transformation parameter. One reason for this could be reliance on Huber estimators of location and scale, which are less robust to outliers than the median and MAD (see Figure S.8), for outlier initialization.

### 3.3.2 Influence of outliers on median and MAD

Why would robust z-scoring fail in even Gaussian data at higher contamination levels, as seen in Figure S.1? To answer this question, we perform a small additional simulation study. Using the same distributions, sample size and outlier contamination levels from the main simulation, we examine the Monte Carlo sampling distributions of the median and MAD. Histograms across 1000 replications of size  $n = 500$  are shown in **Figure S.7** for Gaussian data and for skewed data. In

the Gaussian case, the median remains unbiased as the proportion of outliers grows. However, the MAD scale estimator grows as the number of outliers increases. This is because outliers, as defined here as large-magnitude values, shift a portion of the distribution to the tails. This shifts the quantiles of the absolute differences, and hence the MAD, progressively upwards. In the skewed case, the median also exhibits upward bias as the proportion of outliers increases. This is because in skewed data, here we consider outliers as being large, positive values, which will similarly shift all the quantiles upwards, including the median. This breakdown at higher outlier contamination levels of the MAD, and in skewed distributions the median also, will lead to suboptimal performance of robust z-scoring, and hence of any method that depends on it to initialize outliers.

**Figure S.8** considers several alternative robust estimators of center and scale, including Huber estimators used to initialize outliers in robust Box-Cox/YJ transformation (Raymaekers and Rousseeuw, 2021) and  $Q_n$  and  $S_n$  estimators Rousseeuw and Croux (1993). Across all distributions, the Huber estimators show the least robustness to outliers. This is likely why robust Box-Cox/YJ transformation tends to suffer at moderate-to-high outlier contamination levels. As the percentage of outliers increases, the median exhibits positive bias in all skewed distributions, and the MAD exhibits positive bias in all distributions. The  $Q_n$  and  $S_n$  estimators are more biased than the MAD in symmetric distributions, while  $Q_n$  shows slightly less bias in skewed distributions. Thus, the influence of large-magnitude, possibly asymmetric outliers is a problem for many robust estimators, and seems to be an even greater problem for the alternative estimators to the median and MAD considered here. Any method that relies on robust z-scores to identify or initialize outliers is therefore likely to deteriorate at high outlier contamination levels.

### 3.4 Sensitivity and specificity to outliers

Turning now to quantitative evaluation of the SHASH transformation and existing methods, **Figure 5** shows their TPR and FPR over 1000 simulated datasets for each distribution and outlier contamination level. Both SHASH-z and SHASH-i exhibit strong overall performance, particularly at lower contamination levels. At high contamination (30%), the sensitivity of SHASH-z starts to suffer in Gaussian and skewed distributions, suggesting the influence of outliers on the transformation parameters and poor outlier initialization. By contrast, SHASH-i remains robust even under heavy contamination, outperforming SHASH-z and existing methods in skewed and Gaussian data.

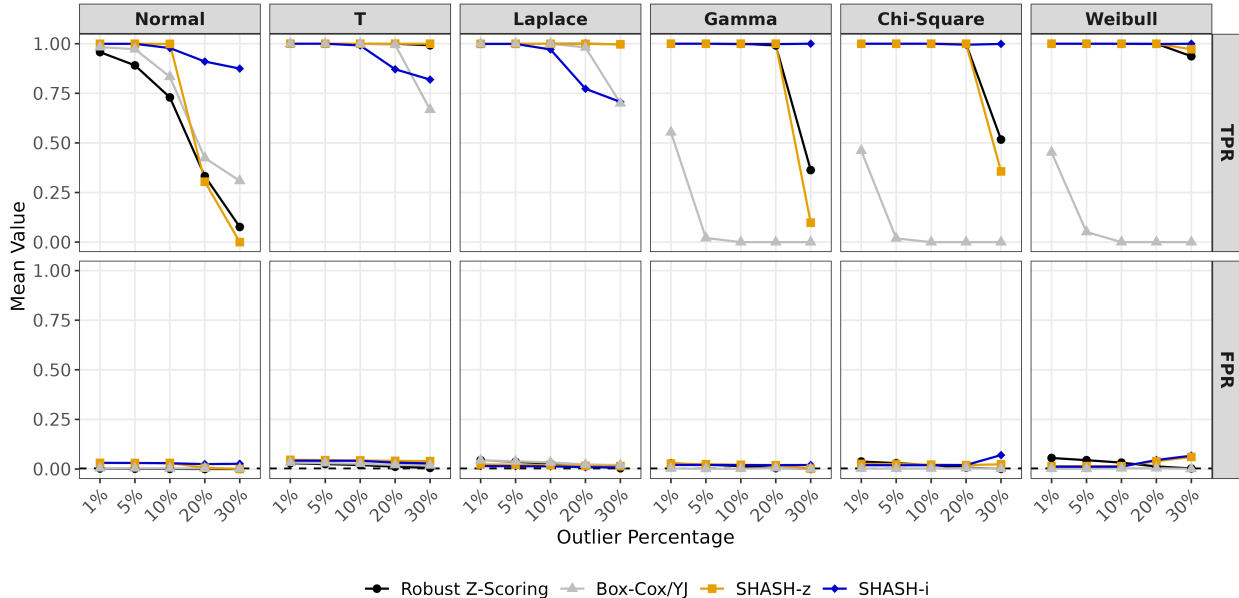


Figure 5: **Accuracy of outlier detection in simulation study.** True positive rate (TPR), i.e. sensitivity, and false positive rate (FPR) (mean over 1000 simulations) across distributions and outlier contamination levels for four robust outlier detection methods: z-scoring, Box-Cox/YJ transformation, SHASH-z and SHASH-i transformations. The horizontal line in the bottom panels indicates the nominal false positive rate of 0.003.

It is, however, outperformed by SHASH-z in heavy tailed distributions with high contamination. In terms of false positives, at low-moderate contamination levels there is no clear winner between robust z-scoring and SHASH transformation (robust Box-Cox/YJ transformation has a near-zero FPR but this is generally due to poor sensitivity). At very high contamination levels the FPR of SHASH-i and SHASH-z increase slightly in some distributions, which is the tradeoff for high sensitivity to outliers.

## 4 Real Data Analysis

We apply robust SHASH transformation and outlier detection, alongside existing methods, to several real-world datasets commonly considered in the outlier detection literature. These datasets represent a wide variety of distribution shapes and contexts. In some cases the outlier identities are known or can be reasoned. Specifically, we consider three datasets:

1. The Top Gear dataset (Alfons, 2019) includes 297 production vehicles featured on the BBC’s Top Gear website, with variables such as engine specifications, fuel economy and performance

metrics. We consider the MPG and Weight variables, which were previously examined by (Raymaekers and Rousseeuw, 2021) to evaluate the performance of robust Box-Cox/YJ transformation. In addition, we consider Price, given its extreme right skew and the presence of several expensive models that can be considered outliers.

2. The HBK dataset is a well-known dataset introduced by Hawkins et al. (1984) consisting of 75 observations on four variables. Fourteen (18.6%) of the observations are known to be outliers (Maechler et al., 2025). Given the number and size of the outliers, they are potentially influential on the transformation, making this dataset particularly susceptible to the masking effect. Since the outlier identities are known, the performance of each method can be assessed.
3. The Wood dataset (Rousseeuw and Leroy, 1987; Maechler et al., 2025) contains 20 observations on five variables related to wood-specific gravity. A noteworthy feature of this dataset is that the distributions exhibit short tails, which the SHASH transformation is uniquely equipped to deal with. These data were contaminated by replacing some observations with outliers, so the outlier identities are known. This data set is analyzed in the principal component space using robust PCA (Hubert et al., 2005) since the outliers are multivariate.

**Figure 6** displays the results for the Top Gear dataset, including histograms before and after transformation using robust Box-Cox/YJ and SHASH transformations. The outlier detection threshold on the original scale of the data is annotated on each transformed histogram. For MPG, all transformations perform reasonably, with SHASH-transformation having a slightly lower outlier detection threshold (78.8 MPG versus 96.3 MPG based on Box-Cox transformation). This results in several additional borderline cases being identified as outliers, including three cars with 80-88 MPG, in addition to the extreme outliers also identified by Box-Cox transformation, with MPG values between 235-470 MPG. Whether or not cars with MPG over 80 should be considered outliers is subjective and depends on the context and data analysis goals. Indeed, these observations would not be labeled as outliers using SHASH with a slightly higher outlier detection threshold of 4 post-transformation. The final outlier detection threshold can and should be determined based on the goals of outlier detection, whether that is to detect all unusual values or simply to identify the most egregious outliers.

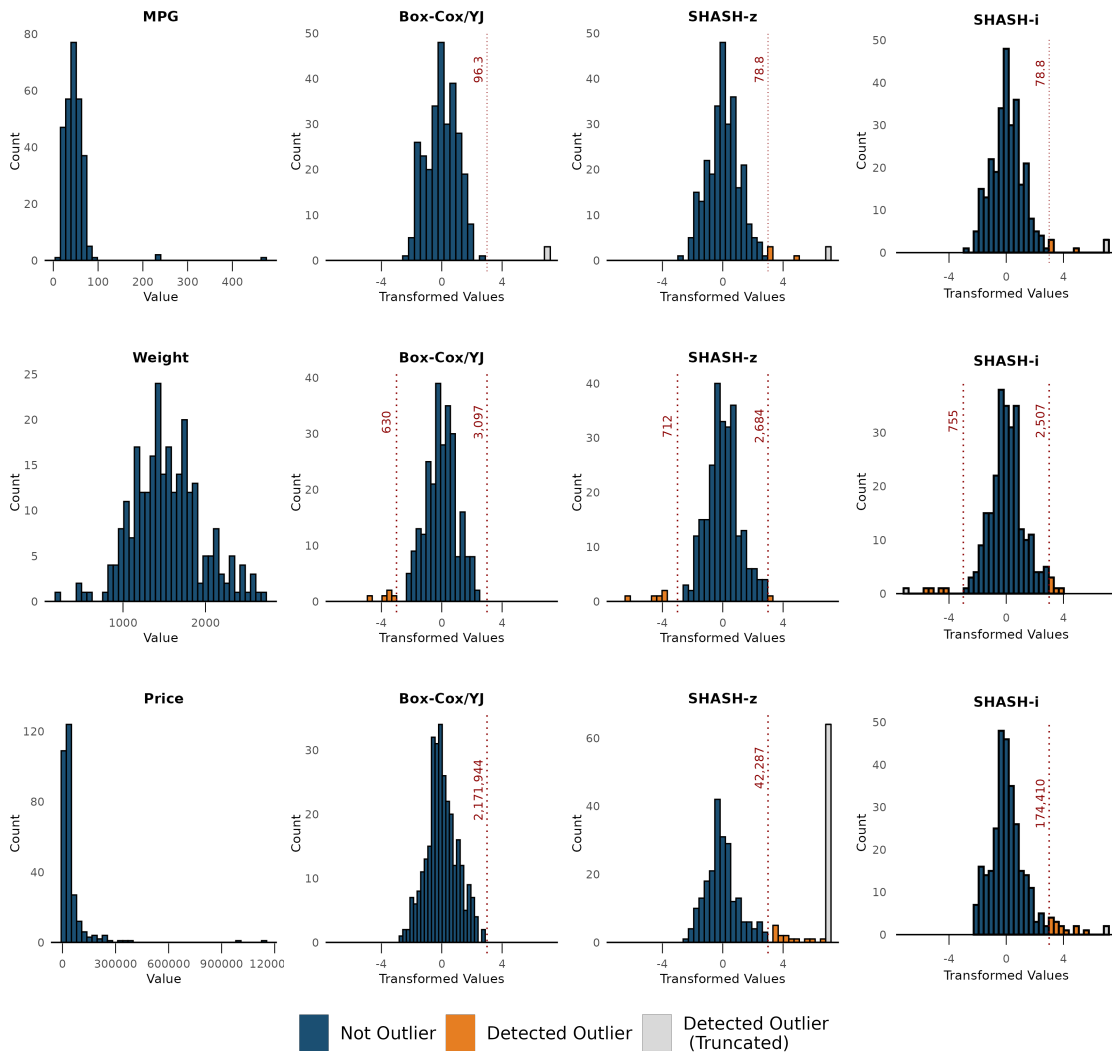


Figure 6: Application of outlier detection methods to three variables from the Top Gear dataset. True outlier identities are unknown; color indicates outlier flags based on each method. Values beyond  $\pm 7$  are truncated for visualization purposes. For each transformation, the outlier detection threshold on the original scale of the data is annotated on the plot.

The second row of **Figure 6** displays histograms of the Top Gear variable Weight before and after transformation. Again both versions of the SHASH transformation are somewhat more conservative than YJ transformation. The latter flags five observations with weight below 630 kg, while SHASH transformation flags these ones in addition to several heavier cars, with weight above approximately 2500 kg. These are again borderline, subjective cases that could be considered outliers or not, depending on the context, and would not be flagged using SHASH with a post-transformation threshold of  $\pm 4$ . Notably, the five outliers in the left tail are more clearly accentuated with SHASH-i compared with YJ or SHASH-z transformation, making them easy to detect even with a higher threshold of  $\pm 4$ .

Turning finally to Price, shown in the bottom row of **Figure 6**, the data is extremely right-skewed, with most cars costing below 100,000 UK pounds (£) but with several costing over £300,000 and two costing approximately £1 million. If any of these outliers are allowed to influence the transformation, masking is very likely to occur. This is the case with Box-Cox transformation, which surprisingly does not flag any outliers and produces a threshold corresponding to £2.17 million. At the other extreme, SHASH-z is overly conservative, with an outlier threshold of only £42,287. SHASH-i, by contrast, results in a reasonable outlier flag of £174,410. Considering the original histogram, this flags all cars in the long right tail, which is clearly distinct from the bulk of the distribution, as well as the two very extreme outliers around 1 million pounds. Therefore, for Price, SHASH-i alone provides a reasonable outlier threshold. As with Weight and MPG, whether or not all of the flagged cars should be considered outliers is subjective, and the outlier detection threshold can be adjusted to reflect the data analysis goals. A SHASH-i threshold of 4, for example, would flag car prices over £256,951 as outliers.

**Figure 7** displays the results of the HBK dataset. In all four variables, there is a distinct cluster of known outliers in the right tail. This dataset provides a good example of the masking effect, since the size and quantity of outliers have the potential to influence the transformation if a non-robust or insufficiently robust procedure is used. Both the Box-Cox and SHASH-i transformation perform well for three of the four variables but fail for one variable, leading to masking of all outliers; SHASH-z performs well on all four variables. This illustrates that while SHASH-i is generally sensitive to outliers due to effective outlier initialization, in some cases it will fail to initialize some outliers, ultimately leading to masking due to the influence of unexcluded outliers on the transformation.

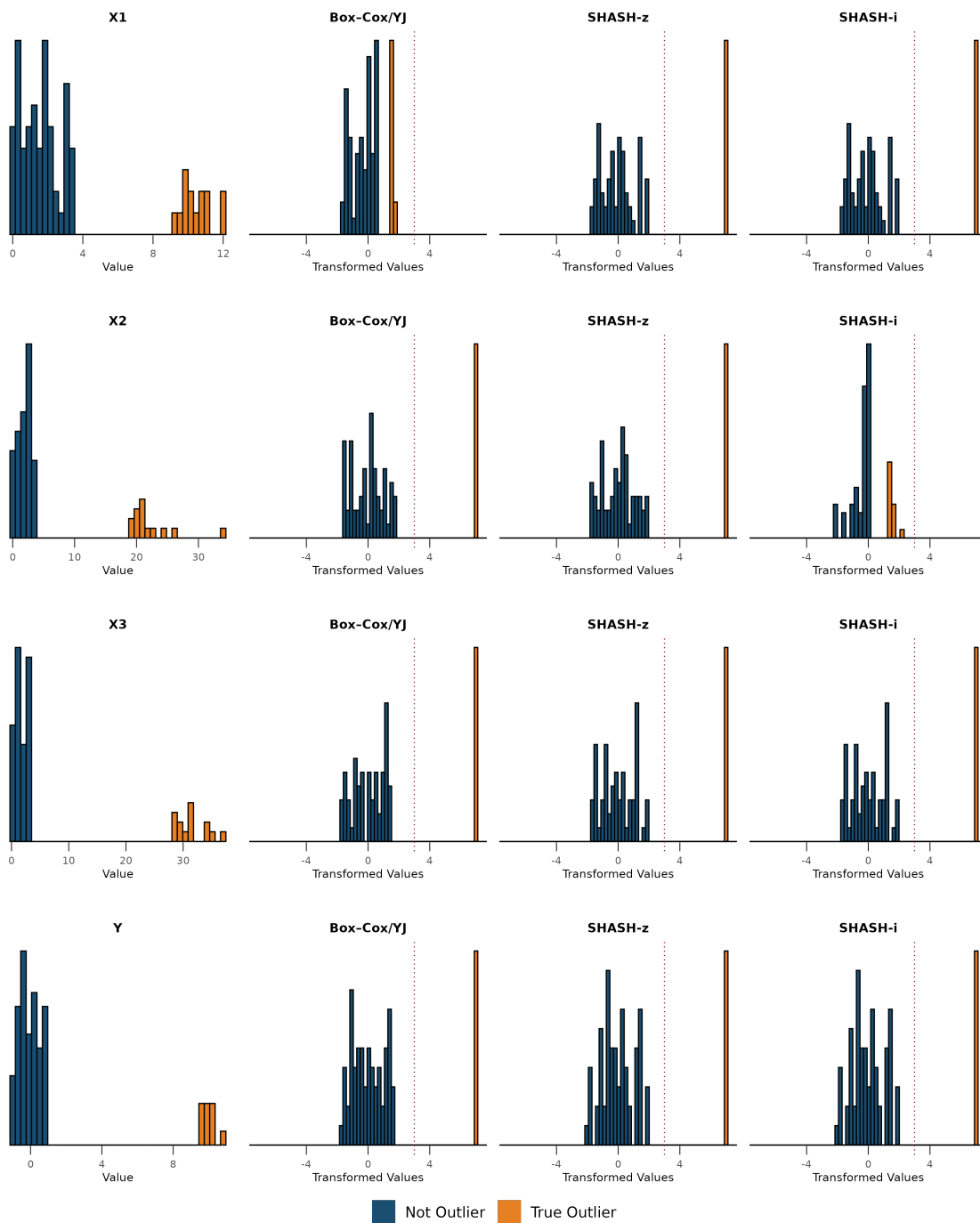


Figure 7: Application of outlier detection methods to four variables in the HBK dataset. True outlier identities are indicated with color. Transformed values are truncated at  $\pm 7$  for visualization purposes.

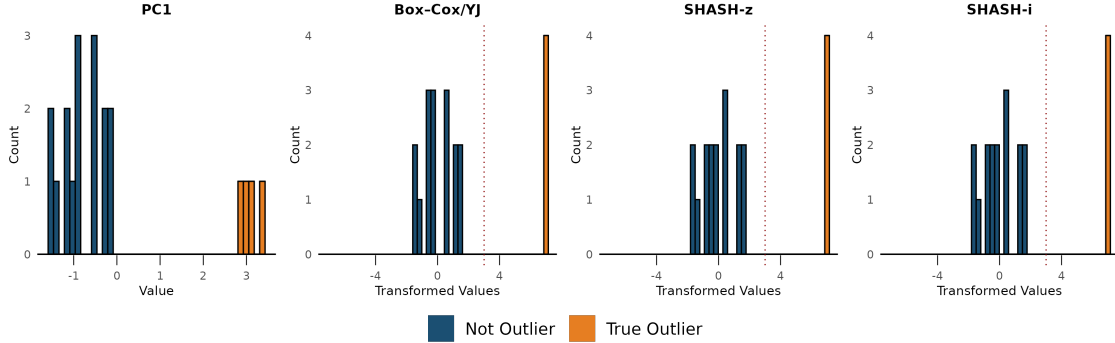


Figure 8: **Application of outlier detection methods to Wood dataset.** The first robust principal component is shown. True outlier identities are indicated with color. Transformed values are truncated at  $\pm 7$  for visualization purposes.

This suggests a potential modification of the outlier initialization underlying SHASH transformation to improve sensitivity to outliers: combine the strengths of SHASH-z and SHASH-i by initializing as outliers any observations identified using either method. Such a combination approach would ensure that if SHASH-z or SHASH-i effectively initializes outliers, masking will likely be avoided.

Lastly, **Figure 8** displays the results of the Wood dataset. A scatterplot matrix among the five variables is shown in Figure S.9, which reveals the several known multivariate (but not univariate) outliers. Figure 8 displays a histogram of the first principal component, which clearly reveals the outliers. All three methods successfully identify the outliers.

## 5 Application to functional neuroimaging

Here, we apply SHASH-based outlier detection in the context of denoising functional neuroimaging data, specifically functional magnetic resonance imaging (fMRI). Functional MRI data is highly sensitive to contamination through head movements, scanner instabilities, physiological signals, and other sources. The conventional approach to detecting fMRI time points or *volumes* contaminated by artifacts is using participant head motion (Power et al., 2012). However, while head motion is a major source of artifacts, relying on it alone has been shown to be suboptimal in terms of sensitivity and specificity (Pham et al., 2023). There is growing recognition of the need for statistically principled outlier detection techniques for automatic detection of contaminated fMRI volumes (Afyouni and Nichols, 2018; Mejia et al., 2017).

We previously developed techniques for extracting low-dimensional features from high-dimensional

fMRI data that are likely to reveal the presence of artifacts (Pham et al., 2023). Specifically, we use spatial independent component analysis (ICA), which is a well-established technique to separate signal and noise in fMRI data (McKeown et al., 1998; Griffanti et al., 2014). Spatial ICA produces a set of spatial maps that are maximally independent and a corresponding set of time courses representing the temporal engagement of each component during the fMRI session. While the ICA components themselves (the spatial maps) are by construction approximately independent, the temporal components have no constraints and tend to exhibit substantial dependence. For the purposes of detecting volumes exhibiting abnormalities, we select the components whose time courses have levels of kurtosis indicating a significant deviation from outlier-free Gaussian data. These components tend to be non-Gaussian given their high kurtosis levels, and in our experience they exhibit a variety of non-Gaussian distributional properties. Hence, in this context there is a need for outlier detection techniques appropriate for non-Gaussian data.

We analyze fMRI data from two participants in the Autism Brain Imaging Data Exchange (ABIDE) initiative (Di Martino et al., 2014). For ease of visualization, we select a single axial slice through the middle of the volume. After applying a brain mask to remove background regions and vectorizing, the data can be represented as a  $T \times V$  matrix, where  $T$  is the number of volumes and  $V$  is the number of in-mask volumetric elements or *voxels*. For these two subjects,  $T = 193$  and  $145$ , and  $V = 4,675$  and  $4,679$ , respectively. Visual inspection of the raw fMRI scans reveals that the first subject’s data contains high levels of artifact-related contamination. The number of high-kurtosis ICA time series is 29 and 24 for subjects 1 and 2, respectively. Since outliers may be multivariate across these components, we first apply robust PCA across the ICA time courses, as in the Wood dataset (Hubert et al., 2005). We retain the PCs explaining 80% of the total variance, resulting in 14 PCs for subject 1 and 13 PCs for subject 2. If a volume is detected as an outlier in any PC, we consider it an outlier.

Applying a final outlier detection threshold of  $\pm 3$ , we detect 68 outlying volumes for the first (high noise) subject and 40 outlying volumes for the second (lower noise) subject. While these numbers may appear high, they are consistent with fMRI volume censoring rates based on stringent motion thresholds (Pham et al., 2023). Using a more lenient outlier detection threshold of  $\pm 4$ , we would detect 43 and 16 outlying volumes, respectively. Whether to use a stringent or lenient outlier detection threshold depends on the data analysis goals and context, and is a matter of substantial

debate in the functional neuroimaging literature (Satterthwaite et al., 2019).

**Figure 9** shows Normal Q-Q plots for the first principal component for each subject before and after SHASH transformation. The distribution for subject 1 exhibits light tails prior to transformation, while the distribution for subject 2 is slightly right-skewed. While several points clearly deviate from the bulk of the distribution prior to SHASH transformation, none exceed the outlier detection threshold of  $\pm 3$ , indicated by the grey band. By contrast, after transformation several observations are identified as outliers. The most extreme outlier in PC1 is volume 60 of subject 1, which is visualized in **Figure 10** along with several neighboring volumes. Its immediately preceding neighbor is also detected as an outlier, while a slightly earlier volume is not. A banding artifact consistent with head motion is clearly seen in the two outlying volumes, while no such abnormalities are seen in the non-outlying volume.

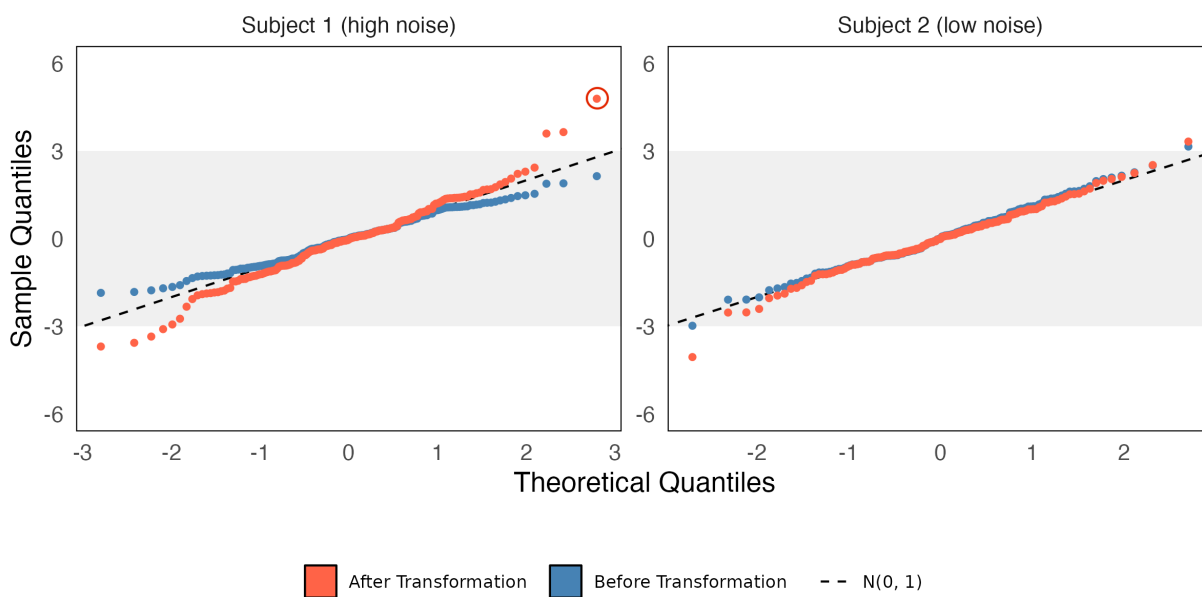


Figure 9: Standard normal QQ plots for the first robust principal component in the ABIDE fMRI datasets. The “before” distribution is robustly centered and scaled to have mean zero and unit variance, and is therefore on a comparable scale. Observations exceeding  $\pm 3$  (gray band) are labeled as outliers for this PC. The circled outlier for subject 1 is volume 60, which is visualized in Figure 10.

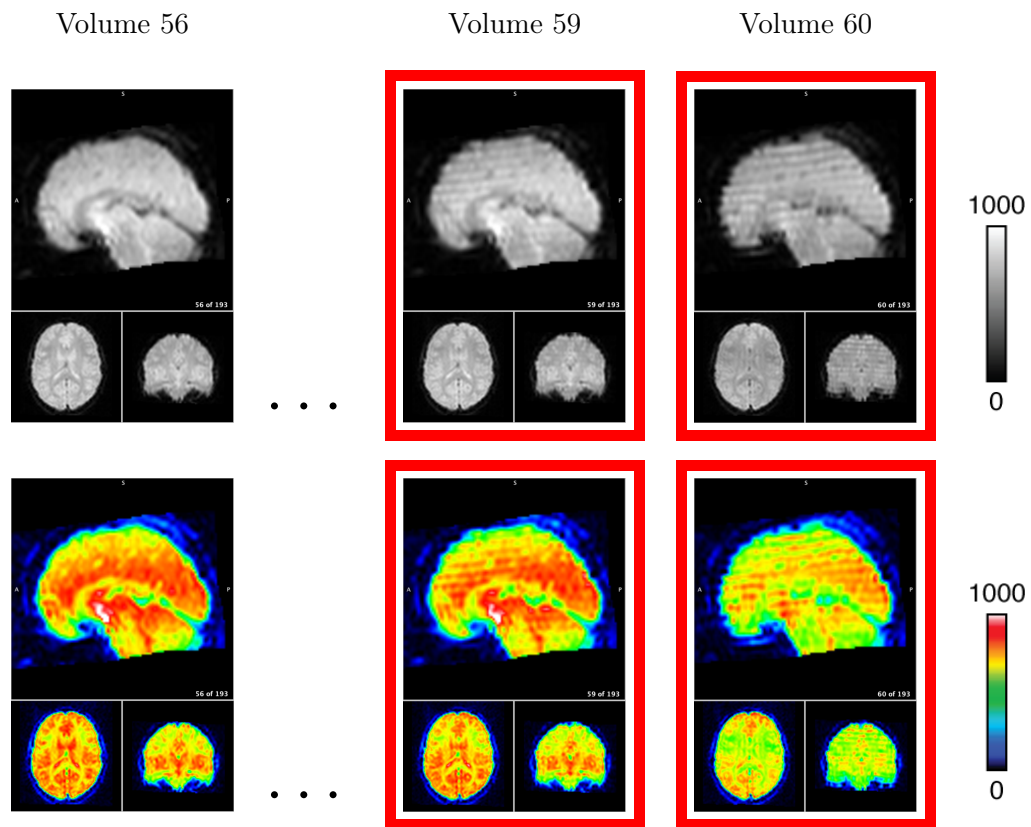


Figure 10: **Visual examples of outlier volumes for ABIDE subject 1.** The first row shows orthogonal views of several volumes in the traditional grayscale, while the second row uses a spectral palette to visually accentuate spatial patterns. Volume 60 (the PC1 outlier circled in Figure 9) and its immediately preceding neighbor are detected as outliers based on a threshold of  $\pm 3$  or  $\pm 4$ , while volume 56 is not detected as an outlier at either threshold. A banding artifact consistent with head motion is clearly seen in volumes 59 and 60, while no such abnormalities are seen in volume 56.

## 6 Discussion

In this work, we have developed a novel robust outlier detection method based on the flexible sinh-arcsinh (SHASH) family of distributions. We developed two variations, which differ in their method of initializing outliers, a crucial step to avoid the undue influence of outliers on the transformation. SHASH-z uses a traditional robust z-score approach for initialization, while SHASH-i uses a novel version of the anomaly detection technique iForest. Through extensive simulation studies and a rich set of real datasets, we benchmarked the performance of SHASH transformation against two existing methods: robust z-scoring and a recently developed robust Box-Cox/YJ transformation. In both simulated and real data settings, SHASH transformation consistently exhibited strong performance.

In heavy tailed distributions, all methods showed good sensitivity to outliers. Even at the highest level of outlier contamination (30%), all z-score based methods maintained nearly perfect sensitivity to outliers with the exception of robust Box-Cox/YJ transformation, which performed well up to 20% contamination. This is likely because on the original scale of the data, true outliers appear further out in the tails in heavy-tailed distributions, so they are easy to initialize or detect using robust z-scoring, which is the basis of all methods except SHASH-i. The performance of SHASH-i suffered at high levels of outlier contamination in heavy tailed distributions.

In skewed distributions, SHASH transformation and robust z-scoring achieved nearly perfect sensitivity up to 20% outlier contamination, while SHASH-i alone maintained this level of performance at 30% contamination. However, robust Box-Cox/YJ performed poorly in all the skewed distributions we considered, even at low levels of outlier contamination (1%, or five of  $n = 500$  observations). This was surprising, since the Box-Cox and YJ transformations are designed to deal with skew. The culprit is not the transformation itself, but rather poor outlier initialization due to the use of Huber estimators of location and scale, which are much less robust to outliers than the median and MAD (as seen in Figure S.8). These results underscore the susceptibility of transformation methods to the influence of outliers and the importance of effective outlier initialization. If outliers are allowed to influence the transformation, this is almost sure to result in masking of outliers after transformation, as we saw in both simulated and real data.

In summary, our simulations showed that SHASH-i tends to perform best in skewed distributions and Gaussian data, while SHASH-z tends to perform best in heavy tailed distributions. Similarly,

our real data analysis results suggest that SHASH-i and SHASH-z compete in terms of sensitivity to outliers. These findings suggest that combining the outlier initialization techniques underlying SHASH-z and SHASH-i may be an effective strategy to further improve sensitivity and avoid the problem of masking, which many outlier detection techniques suffer from.

Our results also underscore the risk of over-reliance on robust z-scoring to initialize or detect outliers. In simulated Gaussian data, robust z-scoring should exhibit ideal performance with good estimators of location and scale. Instead, its performance deteriorates rapidly as outlier contamination increases beyond 1%. The reasons for this are readily apparent by examining the sampling distributions of the median and MAD (Figure S.7). Specifically, the MAD exhibits positive bias in Gaussian data in the presence of outliers (as defined here, as having unusually large magnitude). This problem is also seen in skewed and heavy tailed distributions (Figure S.8). Additionally, in positively-valued distributions where we define outliers as having unusually large magnitude and positive sign, the median exhibits positive bias due to the presence of outliers. The bias is larger for Huber estimators (location and scale), especially at high levels of outlier contamination. Even if there were no bias, the presence of substantial sampling variance would contribute to suboptimal performance of robust z-scoring. This is likely to be a much bigger issue in small samples.

These limitations of robust z-scoring underscore the need for alternative methods for outlier initialization. Our novel variant on iForest, which is tailored for univariate settings where outliers are considered to be defined based on magnitude, is one such alternative. While this approach has high sensitivity to outliers, its specificity is often suboptimal, and future work is needed to refine this approach. Another possibility is to adopt univariate minimum covariance determinant (MCD) estimators of location and scale, which are based on identifying the subset with smallest variance (Hubert and Debruyne, 2010). The MCD scale estimator may indeed be less susceptible to the presence of outliers than the MAD, which is a quantile-based approach. Future work is needed to identify the optimal strategy for outlier initialization prior to robust transformation. Another possible modification of our robust SHASH transformation would be to relax the outlier detection threshold after initial transformation, or use continuous weights, to incorporate more non-outlying observations into the transformation and thus improve specificity.

This study has several limitations. First, our simulation scenarios only considered a fixed sample size ( $n = 500$ ). Sample size will surely have an influence on the performance of all the methods

considered here, given that they all depend on the estimation of transformation parameter(s). This concern may be mitigated by our analysis of a rich variety of real datasets, which contain a range of sample sizes from small ( $n = 20$ ) to large ( $n = 297$ ). Another limitation is the use of different robust location and scale estimators for outlier initialization in the robust Box-Cox/YJ transformation method, which somewhat hinders fair comparison of that transformation to SHASH transformation. However, since that method was originally designed to use Huber estimators, and is implemented as such in the corresponding software, we chose to maintain that choice in order to provide a realistic assessment of its performance. In addition, here we only considered the SHASH transformation, and did not consider other transformations that can handle skew as well as tail weight (Tsai et al., 2017; Goerg, 2015). Future research is needed to provide a comprehensive comparison of different transformations and outlier initialization techniques.

Finally, here we specifically considered the univariate setting. In the future, we plan to embed SHASH transformation in a multivariate outlier detection procedure. For instance, MCD estimators of location and scale are designed for multivariate outlier detection, but the distribution of robust distances based on MCD estimators is only known in the case of multivariate Gaussian data (Hardin and Rocke, 2005). If the individual variables can be transformed to Normality prior to computing the MCD estimators, knowledge of their distribution can be used to detect observations with unusually large distance from the center of the data, i.e. outliers.

Distributional knowledge—of the data as in this work, or of multivariate distances in a multivariate context—is key because it provides an automated way to detect outliers, rather than relying on visual inspection. Automated outlier detection is essential in the context of big data, since visual inspection does not scale beyond a few datasets. Here we illustrate one compelling application in the context of functional neuroimaging data, which consists of hundreds or thousands of images collected on a single subject. Often, head movements or equipment issues induce artifacts into a single image or a cluster of successive images, which can be considered multivariate outliers. These artifacts need to be detected in an automated fashion for all subjects in the study, where the number of subjects may be in the hundreds or even thousands. A formal robust outlier detection approach to this problem is desirable to facilitate accurate artifact detection and removal to improve the quality and reliability of neuroimaging analyses. This current work provides the necessary precursors that can be built upon to achieve that goal.

## Acknowledgments

The authors gratefully acknowledge Peter Rousseeuw and Brian Caffo for their valuable comments and constructive feedback during the preparation of this manuscript. This work is supported by National Institute of Aging (NIA) grant R01AG083919 to A.F.M.

## References

- Afyouni, S. and Nichols, T. E. (2018). Insight and inference for dvars. *Neuroimage*, 172:291–312.
- Alfons, A. (2019). `robusthd`: Robust methods for high-dimensional data. <https://CRAN.R-project.org/package=robustHD>. R package version 0.6.1.
- Box, G. E. and Cox, D. R. (1964). An analysis of transformations. *Journal of the Royal Statistical Society: Series B (Methodological)*, 26(2):211–243.
- Chabchoub, Y., Akermi, I., and Gargouri, F. (2022). An in-depth study and improvement of isolation forest. *IEEE Access*, 10:17802–17818.
- Di Martino, A., Yan, C.-G., Li, Q., Denio, E., Castellanos, F. X., Alaerts, K., Anderson, J. S., Assaf, M., Bookheimer, S. Y., Dapretto, M., et al. (2014). The autism brain imaging data exchange: towards a large-scale evaluation of the intrinsic brain architecture in autism. *Molecular psychiatry*, 19(6):659–667.
- Donoho, D. L. (1982). Breakdown properties of multivariate location estimators. Technical report, Technical report, Harvard University, Boston. URL <http://www-stat.stanford.edu/>
- Goerg, G. M. (2015). The lambert way to gaussianize heavy-tailed data with the inverse of tukey’s h transformation as a special case. *The Scientific World Journal*, 2015:909231.
- Griffanti, L., Salimi-Khorshidi, G., Beckmann, C. F., Auerbach, E. J., Douaud, G., Sexton, C. E., Zsoldos, E., Ebmeier, K. P., Filippini, N., Mackay, C. E., et al. (2014). Ica-based artefact removal and accelerated fmri acquisition for improved resting state network imaging. *Neuroimage*, 95:232–247.

- Hampel, F. R. (1974). The influence curve and its role in robust estimation. Journal of the American statistical association, 69(346):383–393.
- Hardin, J. and Rocke, D. M. (2005). The distribution of robust distances. Journal of Computational and Graphical Statistics, 14(4):928–946.
- Hawkins, D. M. (1980). Identification of outliers, volume 11. Springer.
- Hawkins, D. M., Bradu, D., and Kass, G. V. (1984). Location of several outliers in multiple regression: Effects of leverage points. Technometrics, 26(3):197–208.
- Hubert, M. and Debruyne, M. (2010). Minimum covariance determinant. Wiley interdisciplinary reviews: Computational statistics, 2(1):36–43.
- Hubert, M., Rousseeuw, P. J., and Vanden Branden, K. (2005). Robpca: A new approach to robust principal component analysis. Technometrics, 47(1):64–79.
- Jones, M. C. and Pewsey, A. (2009). Sinh-arcsinh distributions. Biometrika, 96(4):761–780.
- Liu, F. T., Ting, K. M., and Zhou, Z.-H. (2008). Isolation forest. In 2008 Eighth IEEE International Conference on Data Mining, pages 413–422. IEEE.
- Maechler, M., Rousseeuw, P., Croux, C., Todorov, V., Ruckstuhl, A., Salibian-Barrera, M., Verbeke, T., Koller, M., Conceicao, E. L. T., and di Palma, M. A. (2025). robustbase: Basic robust statistics. R package version 0.99-6.
- Maronna, R. A. (1976). Robust m-estimators of multivariate location and scatter. The annals of statistics, pages 51–67.
- Maronna, R. A. and Zamar, R. H. (2002). Robust estimates of location and dispersion for high-dimensional datasets. Technometrics, 44(4):307–317.
- McKeown, M. J., Makeig, S., Brown, G. G., Jung, T.-P., Kindermann, S. S., Bell, A. J., and Sejnowski, T. J. (1998). Analysis of fMRI data by blind separation into independent spatial components. Human brain mapping, 6(3):160–188.

- Mejia, A. F., Nebel, M. B., Eloyan, A., Caffo, B., and Lindquist, M. A. (2017). Pca leverage: outlier detection for high-dimensional functional magnetic resonance imaging data. Biostatistics, 18(3):521–536.
- Pham, D. Đ., McDonald, D. J., Ding, L., Nebel, M. B., and Mejia, A. F. (2023). Less is more: balancing noise reduction and data retention in fmri with data-driven scrubbing. NeuroImage, 270:119972.
- Power, J. D., Barnes, K. A., Snyder, A. Z., Schlaggar, B. L., and Petersen, S. E. (2012). Spurious but systematic correlations in functional connectivity mri networks arise from subject motion. Neuroimage, 59(3):2142–2154.
- Raymaekers, J. and Rousseeuw, P. J. (2021). Transforming variables to central normality. Machine Learning, pages 1–23.
- Rigby, R. A., Stasinopoulos, M. D., Heller, G. Z., and De Bastiani, F. (2019). Distributions for modeling location, scale, and shape: Using GAMLSS in R. CRC press.
- Rousseeuw, P. J. (1984). Least median of squares regression. Journal of the American statistical association, 79(388):871–880.
- Rousseeuw, P. J. and Croux, C. (1993). Alternatives to the median absolute deviation. Journal of the American Statistical association, 88(424):1273–1283.
- Rousseeuw, P. J. and Driessen, K. V. (1999). A fast algorithm for the minimum covariance determinant estimator. Technometrics, 41(3):212–223.
- Rousseeuw, P. J. and Hubert, M. (2011). Robust statistics for outlier detection. Wiley interdisciplinary reviews: Data mining and knowledge discovery, 1(1):73–79.
- Rousseeuw, P. J. and Leroy, A. M. (1987). Robust Regression and Outlier Detection. John Wiley & Sons.
- Ruppert, D. (2010). Statistics and Data Analysis for Financial Engineering. Springer. p. 118. Retrieved 2015-08-27.

- Satterthwaite, T. D., Ciric, R., Roalf, D. R., Davatzikos, C., Bassett, D. S., and Wolf, D. H. (2019). Motion artifact in studies of functional connectivity: Characteristics and mitigation strategies. Human brain mapping, 40(7):2033–2051.
- Tsai, A. C., Liou, M., Simak, M., and Cheng, P. E. (2017). On hyperbolic transformations to normality. Computational Statistics and Data Analysis, 115:250–266.
- Tukey, J. W. (1957). On the comparative anatomy of transformations. The Annals of Mathematical Statistics, pages 602–632.
- Yeo, I.-K. and Johnson, R. A. (2000). A new family of power transformations to improve normality or symmetry. Biometrika, 87(4):954–959.

## A Derivation of SHASH density

The sinh–arcsinh transformation is defined as

$$Z = S_{\nu,\tau}(X) = \sinh(\tau \sinh^{-1}(X) - \nu),$$

and the inverse sinh–arcsinh transformation is given by

$$X = S_{\nu,\tau}^{-1}(Z) = \sinh\left(\frac{\sinh^{-1}(Z) + \nu}{\tau}\right)$$

Hence, if  $Z \sim N(0, 1)$ , then  $X = Z = S_{\nu,\tau}(X)$  follows a sinh–arcsinh (SHASH) distribution. When location and scale parameters are introduced, the transformation extends to the four-parameter SHASH random variable, which often denoted as SHASHo2), defined as

$$Z = S_{\nu,\tau}(X) = \sinh\left(\tau \sinh^{-1}\left(\frac{X - \mu}{\sigma}\right) - \nu\right)$$

, where  $\mu$  and  $\sigma$  represent mean (location) and standard deviation (scale), respectively. Finally, by reparameterizing the scale as  $\sigma \cdot \tau$ , which helps disentangle the effects of skewness and kurtosis from

the overall scale of the distribution, we obtain the SHASHo2 form:

$$Z = S_{\nu,\tau}(X) = \sinh\left(\tau \sinh^{-1}\left(\frac{X - \mu}{\sigma \cdot \tau}\right) - \nu\right).$$

To derive the probability density function of the SHASHo2 distribution, we apply the change-of-variables rule. Let  $Z \sim N(0, 1)$  with standard normal density  $\phi(Z) = \frac{1}{\sqrt{(2\pi)}} \exp\left(-\frac{z^2}{2}\right)$ . Since the sinh-arcsinh transformation is  $Z = S_{\nu,\tau}(X) = \sinh\left(\tau \sinh^{-1}\left(\frac{X - \mu}{\sigma \cdot \tau}\right) - \nu\right)$ , the corresponding density of  $X$  is obtained as

$$f_X(x) = \phi(Z(X)) \left| \frac{dz}{dx} \right|$$

Define

$$u = \sinh^{-1}\left(\frac{X - \mu}{\sigma \tau}\right), \quad g = \tau u - \nu, \quad Z(X) = \sinh(g).$$

Then, differentiating  $Z(X)$  with respect to  $X$  gives

$$\frac{dZ}{dX} = \cosh(g) \frac{dg}{dX} = \cosh(g) \tau \frac{du}{dX} = \cosh(g) \tau \frac{1}{\sigma \sqrt{1 + \left(\frac{X - \mu}{\sigma \tau}\right)^2}}$$

Substituting into the change-of-variables formula gives

$$f_X(X|\mu, \sigma, \nu, \tau) = \frac{\tau}{\sigma \sqrt{1 + \left(\frac{X - \mu}{\sigma \tau}\right)^2}} \cosh\left(\tau \sinh^{-1}\left(\frac{X - \mu}{\sigma \tau}\right) - \nu\right) \phi\left(\sinh\left[\tau \sinh^{-1}\left(\frac{X - \mu}{\sigma \tau}\right) - \nu\right]\right).$$

To express the pdf in exponential form, let  $w = (X - \mu)/(\sigma\tau)$ , and define

$$r(x) = \sinh(\tau \sinh^{-1}(w) - \nu), \quad c(x) = \cosh(\tau \sinh^{-1}(w) - \nu).$$

Using the following hyperbolic identities

$$\sinh(y) = \frac{e^y - e^{-y}}{2}, \quad \cosh(y) = \frac{e^y + e^{-y}}{2}$$

we can express  $r(x)$  and  $c(x)$  in exponential form as

$$r(x) = \frac{1}{2} [\exp(\tau \sinh^{-1}(w) - \nu) - \exp(-(\tau \sinh^{-1}(w) - \nu))],$$

$$c(x) = \frac{1}{2} [\exp(\tau \sinh^{-1}(w) - \nu) + \exp(-(\tau \sinh^{-1}(w) - \nu))].$$

Hence, the density of the SHASHo2 distribution can be written as

$$f_X(x; \mu, \sigma, \nu, \tau) = \frac{\tau c(x)}{\sigma \sqrt{1+w^2}} \frac{1}{\sqrt{2\pi}} \exp\left[-\frac{1}{2}r(x)^2\right].$$

## B Supplemental Figures

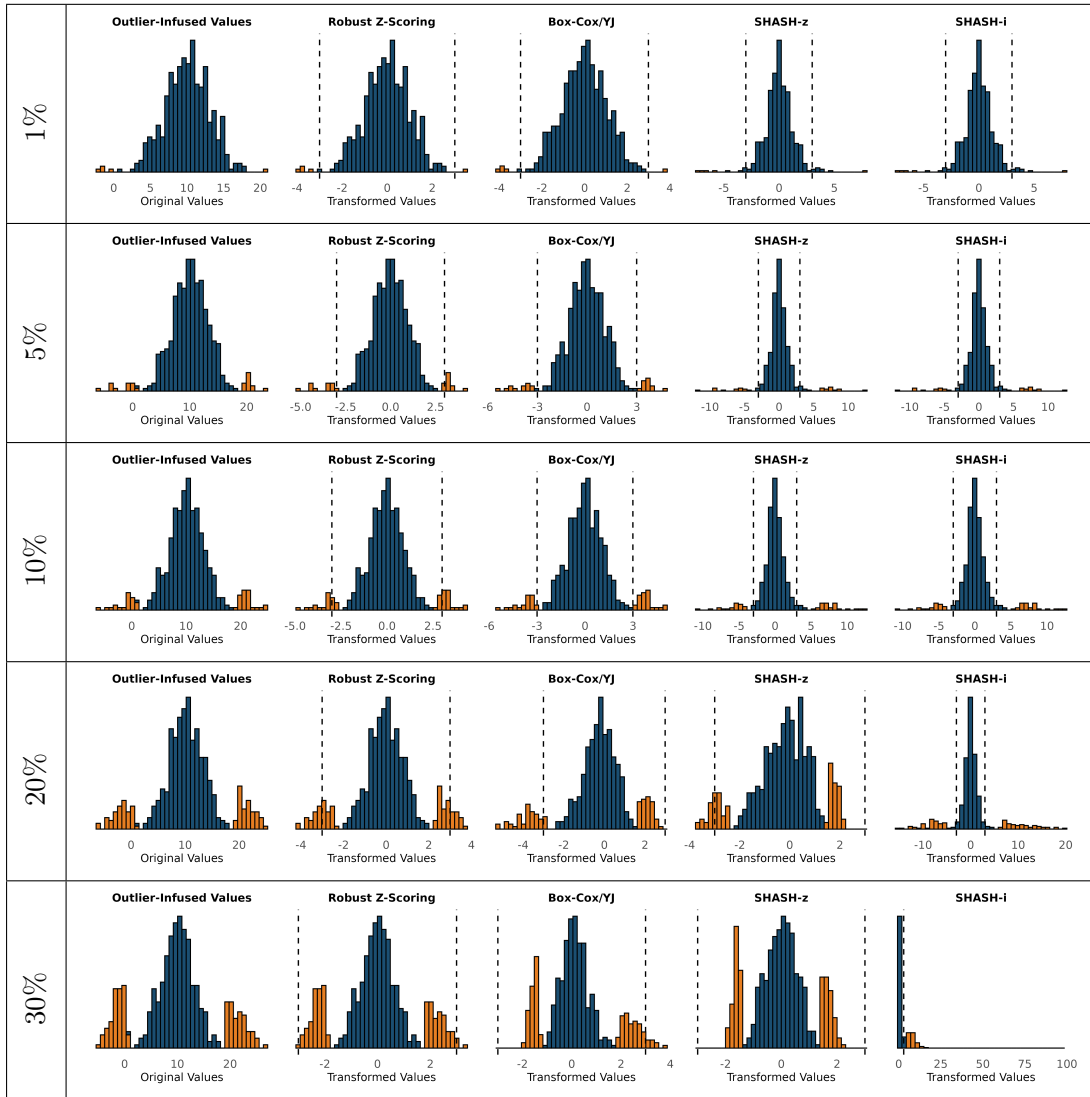


Figure S.1: Histograms of Normal distribution and its transformation to normality using different methods used in the simulations across varying thresholds.

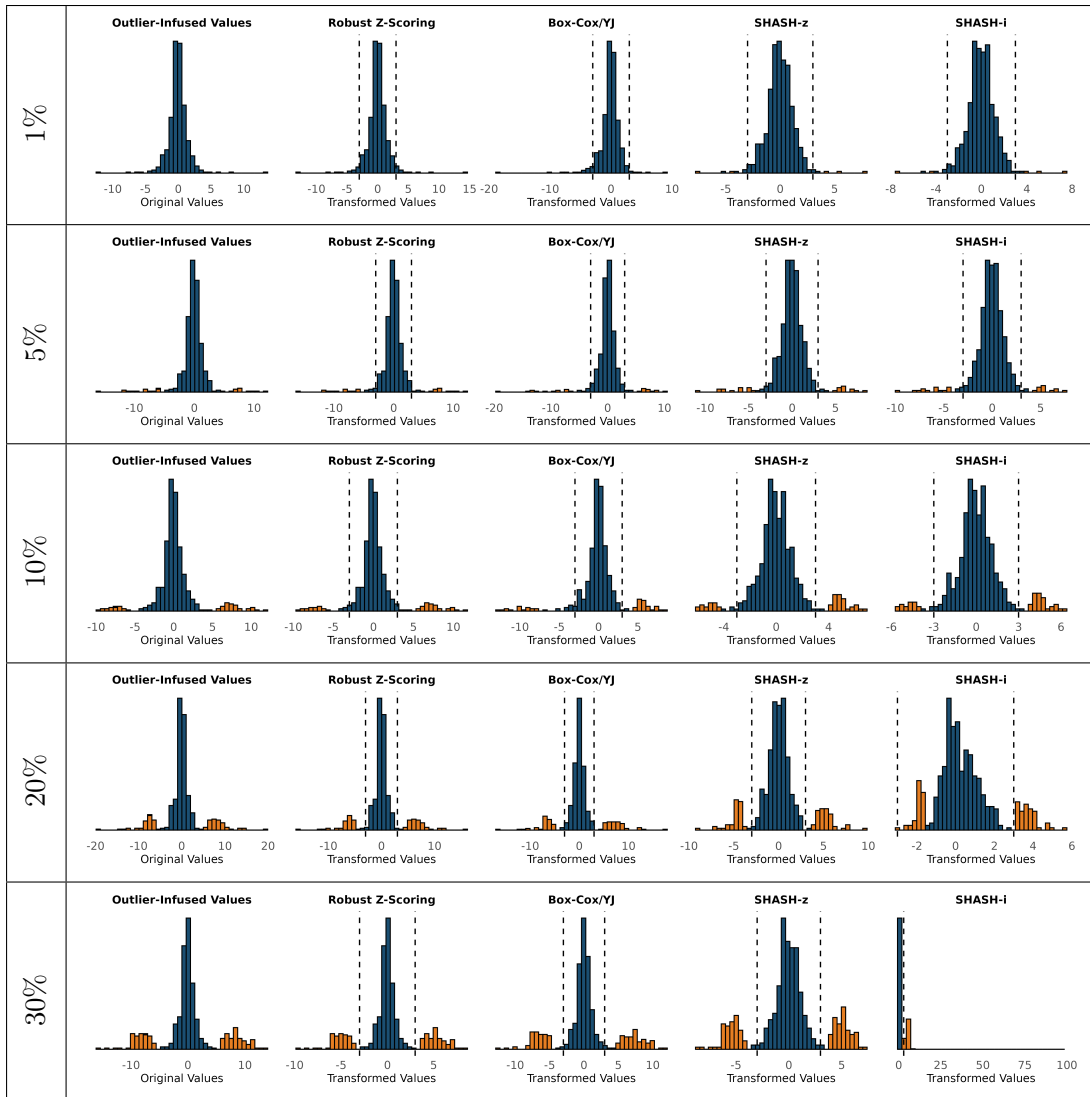


Figure S.2: Histograms of T distribution and its transformation to normality using different methods used in the simulations across varying thresholds.

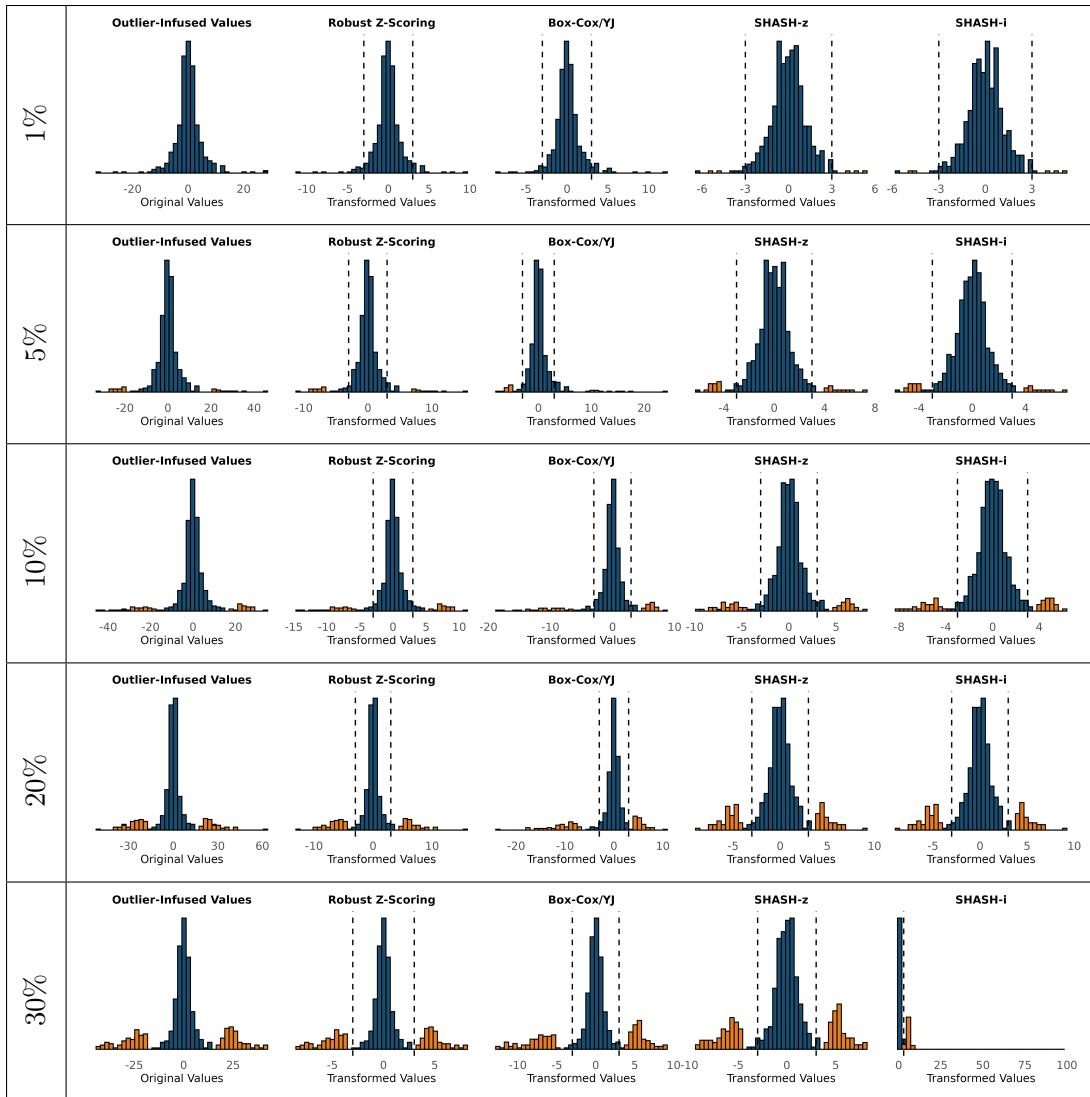


Figure S.3: Histograms of Laplace distribution and its transformation to normality using different methods used in the simulations across varying thresholds.

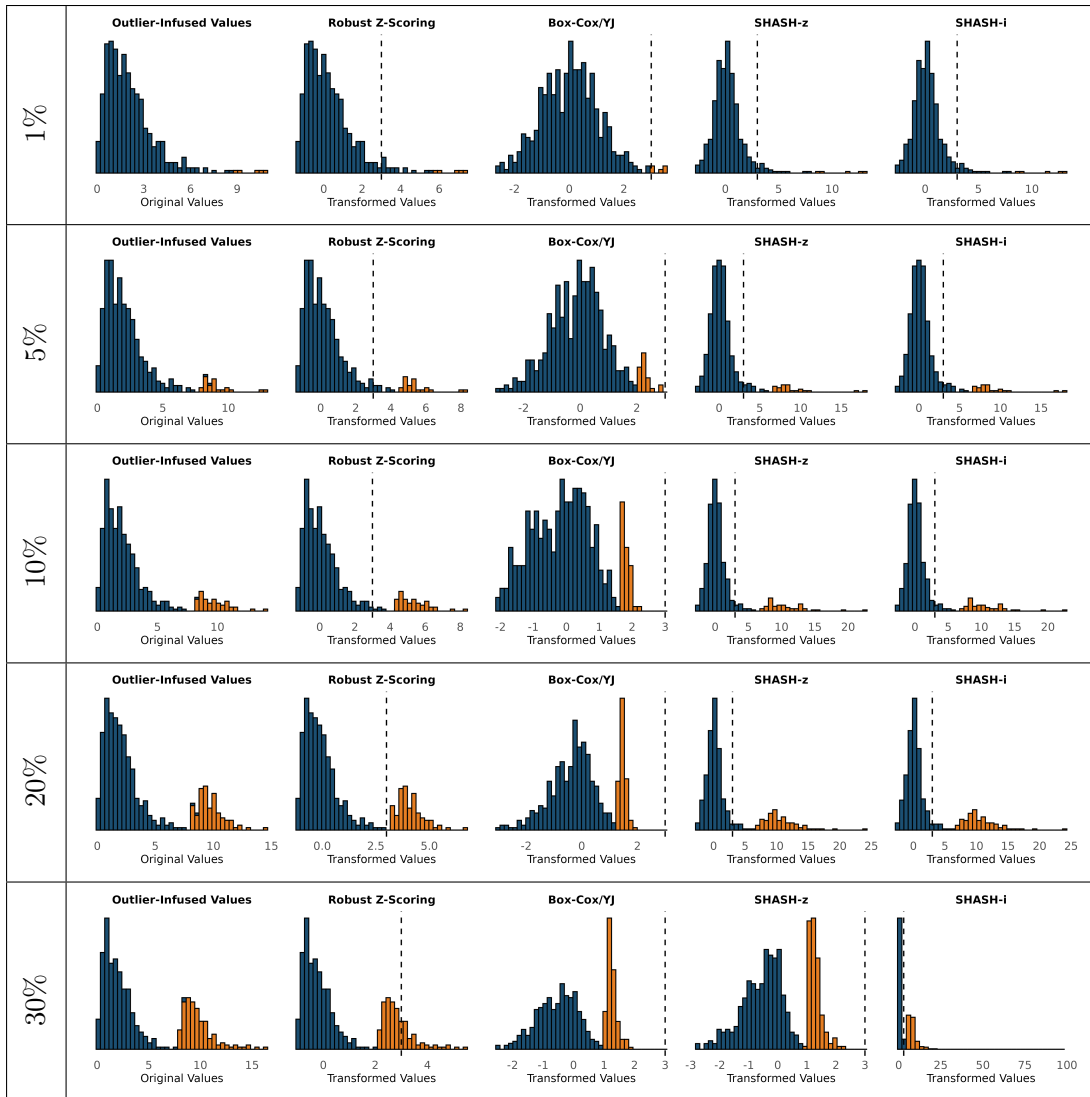


Figure S.4: Histograms of Gamma distribution and its transformation to normality using different methods used in the simulations across varying thresholds.

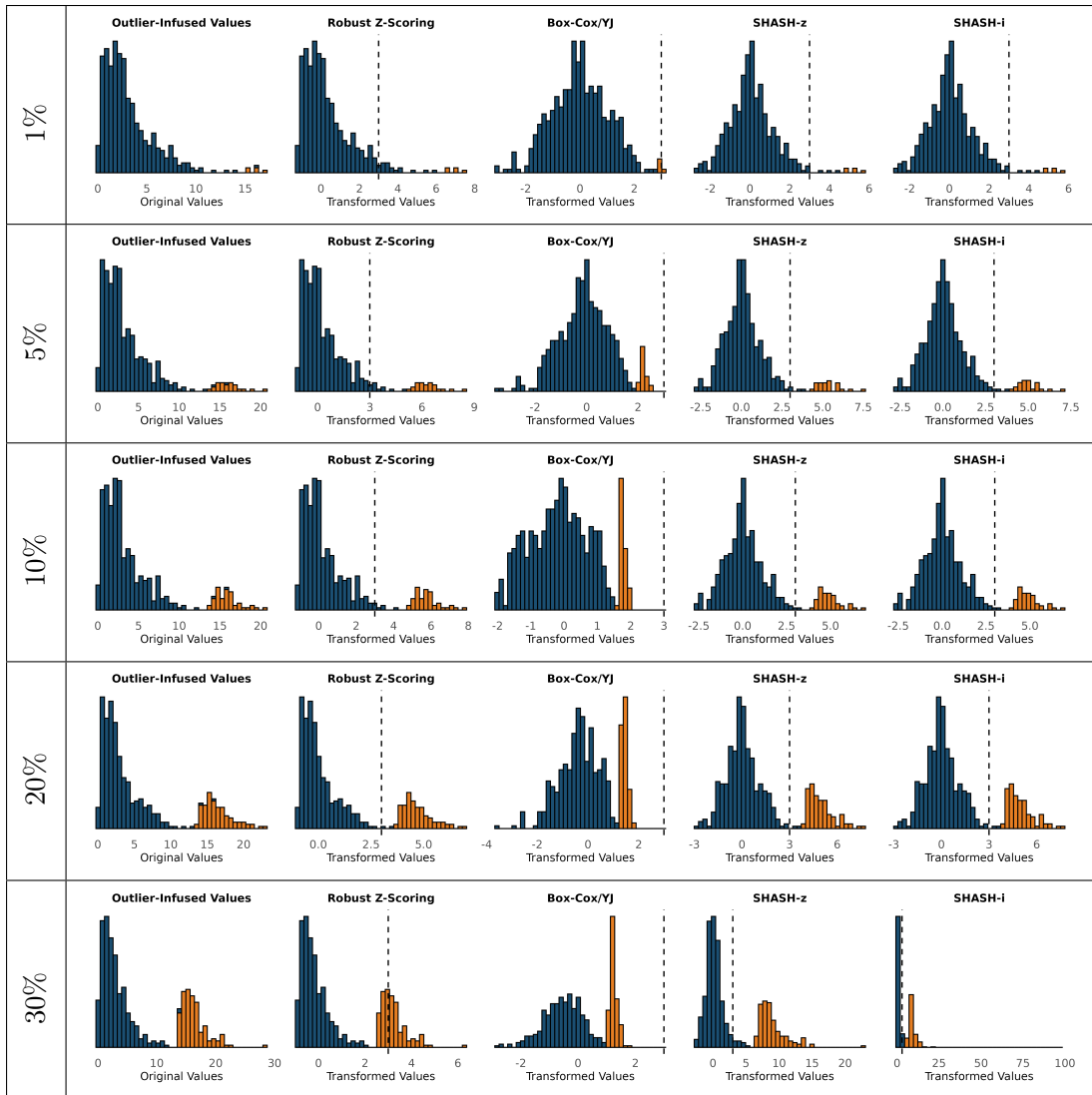


Figure S.5: Histograms of Chi-Square distribution and its transformation to normality using different methods used in the simulations across varying thresholds.

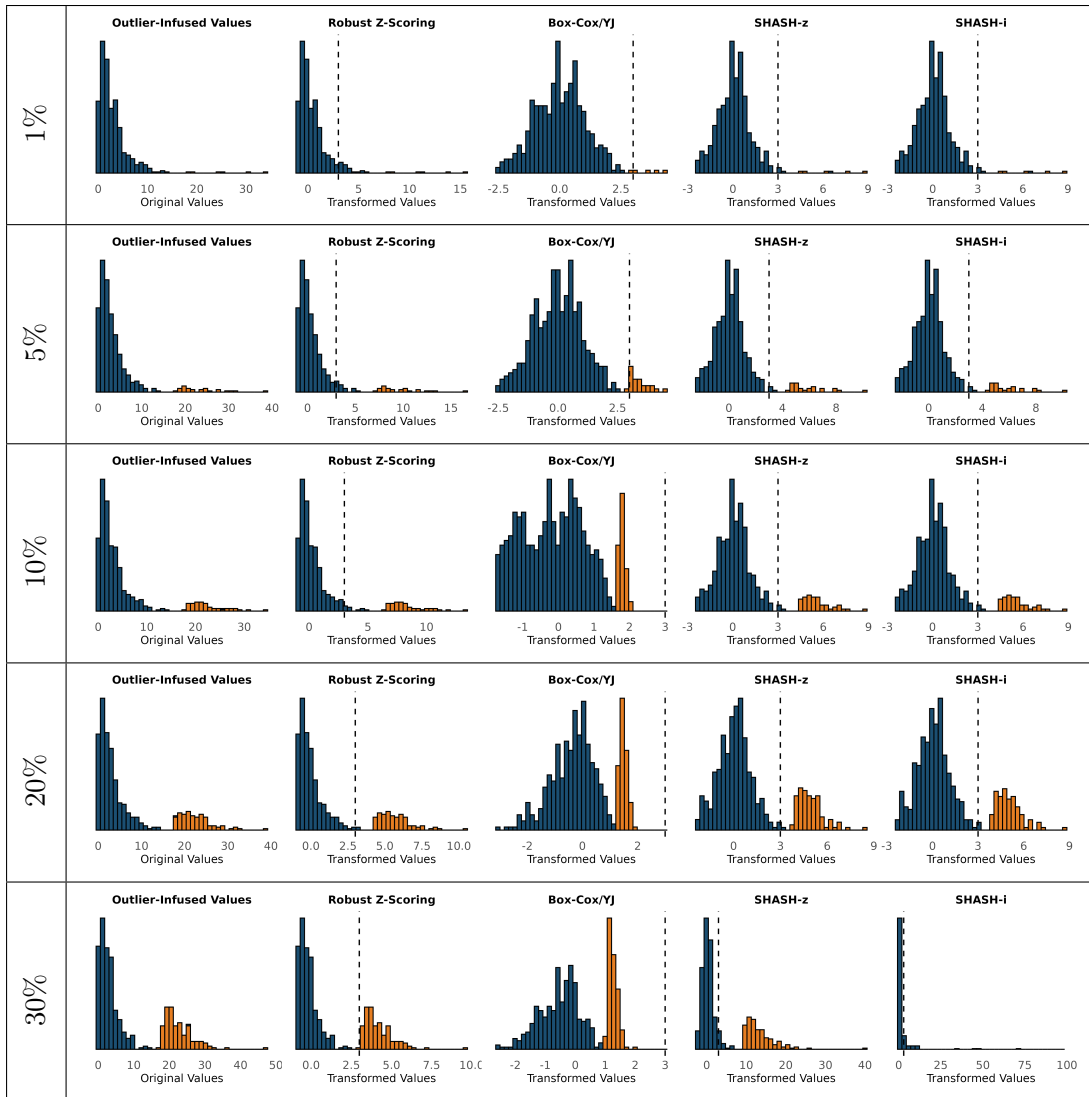


Figure S.6: Histograms of Weibull distribution and its transformation to normality using different methods used in the simulations across varying thresholds. Values over 50 are truncated for visualization purposes.

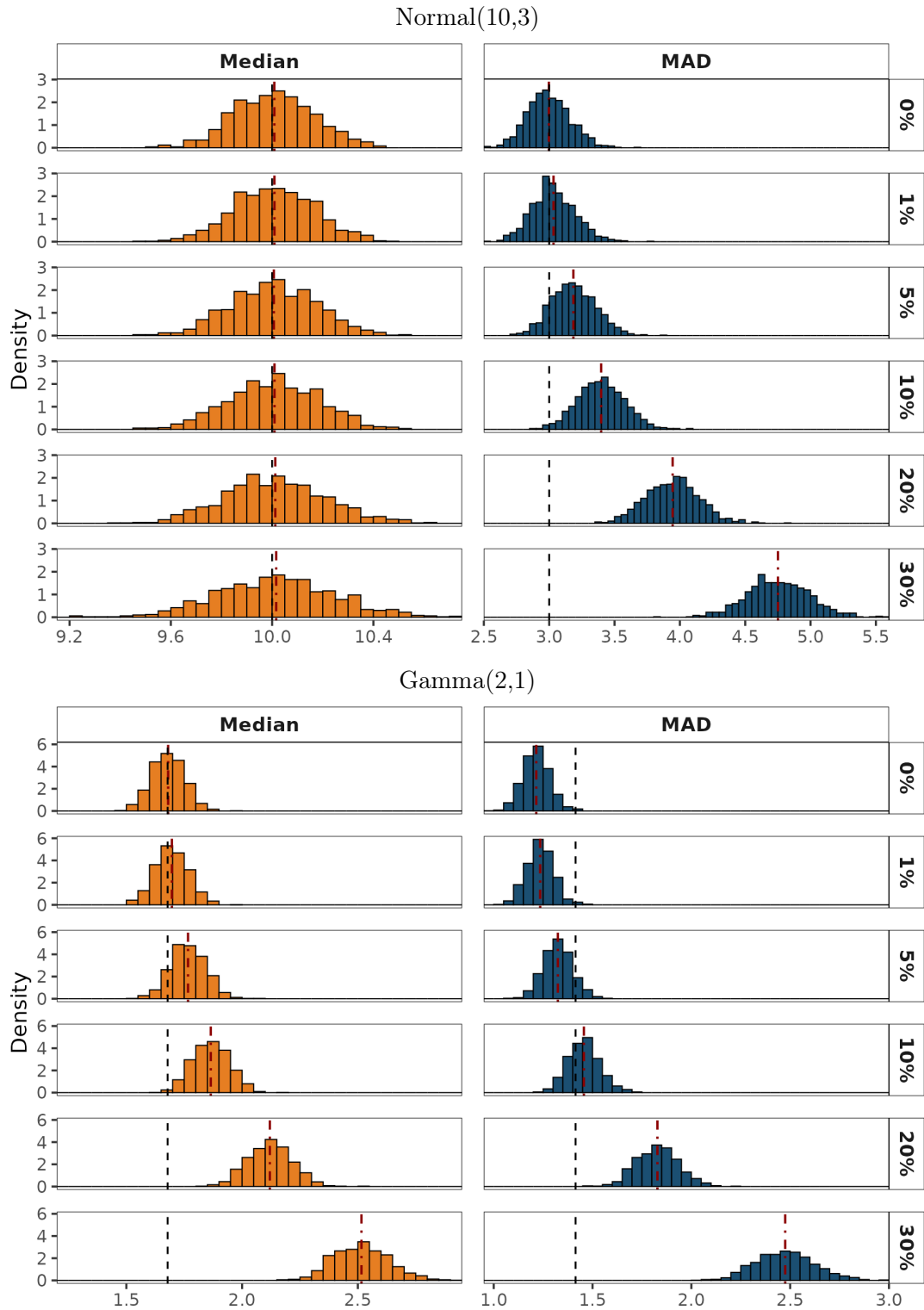


Figure S.7: **Empirical sampling distributions of the median and MAD estimates by outlier contamination level.** The Normal and Gamma distributions are shown to give an example of a symmetric and a skewed distribution. Dark Red dot dash lines represent the sampling distribution mean, while the black dashed lines indicate the true median and MAD values. In the symmetric case, the median remains unbiased, while it is positively biased in the right-skewed case due to the location of outliers in the upper tail. The MAD is upwardly biased in both cases, as regular observations become extreme values, shifting the location of the median deviation upwards.

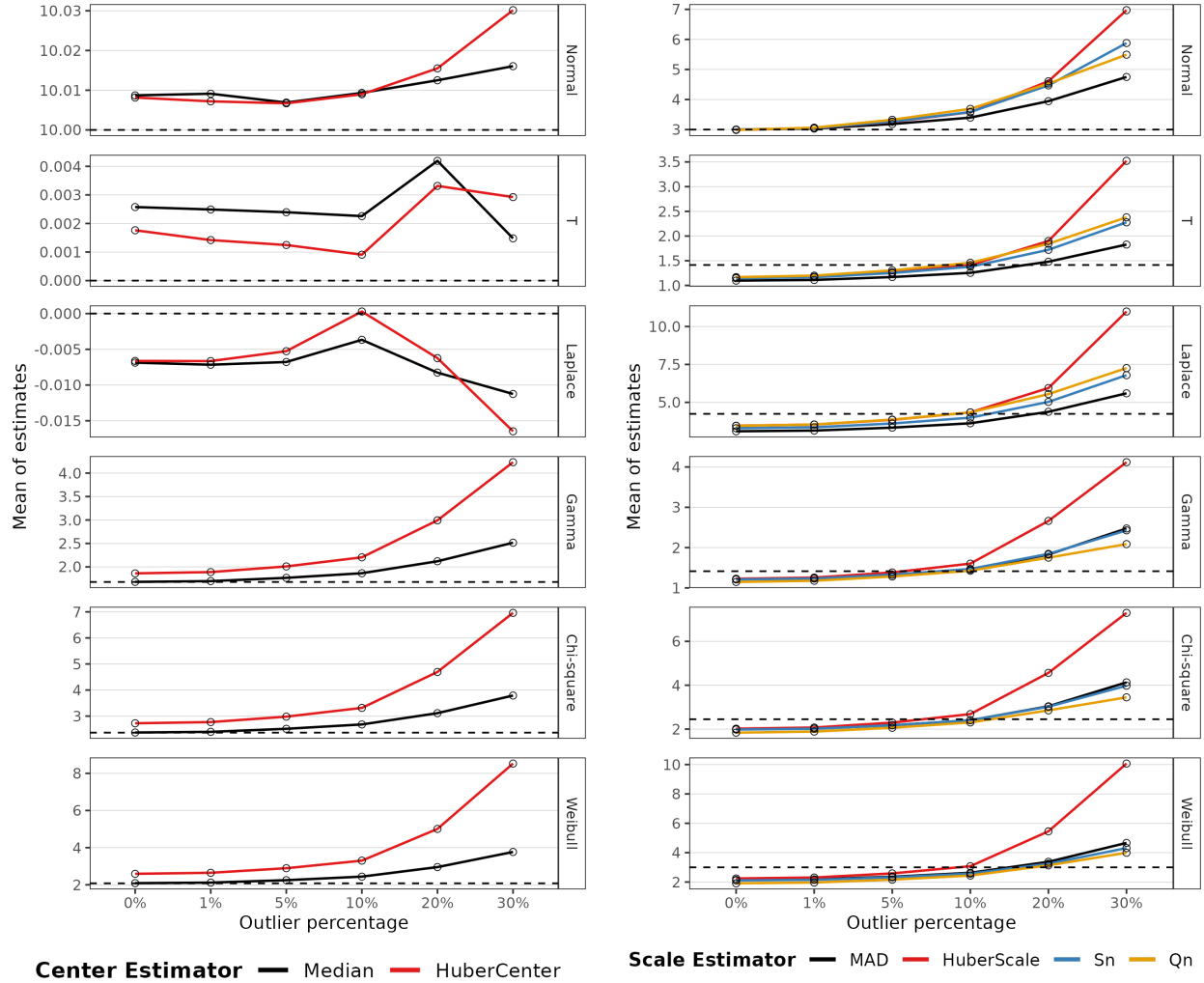


Figure S.8: **Robust estimator performance across contamination levels.** Panel A shows average **center** estimates (Median, HuberCenter) with its legend below; Panel B shows average **scale** estimates (MAD,  $S_n$ ,  $Q_n$ , HuberScale) with its own legend. Black dashed and dotted lines indicate the true population median and standard deviation, respectively.

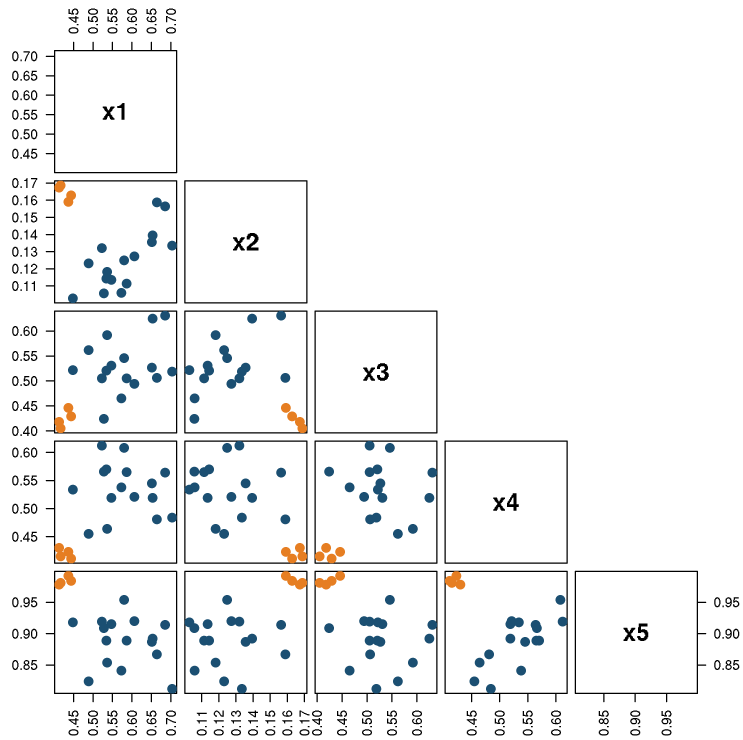


Figure S.9: **Wood dataset – Pairwise scatterplot matrix.** Each panel shows pairwise relationships between predictors in the Wood dataset, with true outliers (observations 4, 6, 8, and 19) highlighted in red.